Turkish Journal of Earth Sciences

Volume 31 | Number 1 Article 6

1-1-2022

Tectonic and structural characteristics of Erzurum and its surroundings(Eastern Turkey): a detailed comparison between different geophysical parameters

ÇAĞLAR ÖZER

SERKAN ÖZTÜRK

EREN PAMUK

TÜBİTAK

Turkish Journal of Earth Sciences

http://journals.tubitak.gov.tr/earth/

Research Article

Turkish J Earth Sci
(2022) 31: 85-108

doi:10.3906/yer-2106-18

Tectonic and structural characteristics of Erzurum and its surroundings (Eastern Turkey): a detailed comparison between different geophysical parameters

Çağlar ÖZER[1,2], Serkan ÖZTÜRK[3], Eren PAMUK[4,*]

[1]Earthquake Research Centre, Atatürk University, Erzurum, Turkey
[2]Department of Civil Engineering, Engineering Faculty, Atatürk University, Erzurum, Turkey
[3]Department of Geophysics, Faculty of Engineering and Natural Sciences, Gümüşhane University, Gümüşhane, Turkey
[4]Department of Geophysical Research, General Directorate of the Mineral Research & Exploration of Turkey, Ankara, Turkey

Received: 21.06.2021 • **Accepted/Published Online:** 15.11.2021 • **Final Version:** 28.01.2022

Abstract: The tectonic and structural properties of Erzurum and its surroundings have been investigated by evaluating the seismo-tectonic *b* - value, magnetic anomaly, edge detection analysis (total horizontal derivative (THDR) and tilt angle (TA)), Curie Point Depth (CPD), P-wave velocity (Vp), and Vp / Vs (S - wave velocity) ratio and by imaging the regional distributions of these parameters. For this purpose, all parameters have been combined to be able to reveal the new useful results on the study region and are presented for different locations and depths. The Vp values have been accompanied by high Vp / Vs ratios and shallow CPD values in the areas with geothermal regions such as Tekman, Söylemez, and the northern part of Karlıova. In the tectonically active regions such as Ilıca, Dumlu, Pasinler, Çat, Karlıova and Karaçoban, high reduction - to – the - pole (RTP) total magnetic anomaly was accompanied by low Vp values in harmony. Besides, the low Vp values between 0 and 10 km and high *b* - values can be related to the weakness zones and the areas in which earthquake hazards are high in the study area. The low Vp values in the 0 km horizontal slice are in accordance with the high RTP total magnetic anomaly values in the triangle area between Aşkale, Ilıca - Dumlu - Pasinler, Narman, and Karaçoban. Uniformly, high Vp and low RTP total magnetic anomaly inclusions overlap in Çat and Tekman. In some regions such as Dumlu, Narman, Horasan, Karaçoban and south of Karlıova, the tilt angle values are positive (positive values in the tilt angle map correspond to the center of the structure causing the magnetic anomaly) and the Vp values are low, but there is not a complete harmony between these parameters. These results show that variations on these parameters are related to each other, and these types of geophysical data are required for tectonic and structural features at different locations and depth levels.

Key words: Vp, Vp / Vs ratio, *b* - value, geothermal, Curie point depth, edge detection

1. Introduction

Erzurum, one of the largest cities in the Eastern Anatolian Region (EAR), has distinct importance due to its renewable energy resources. Geothermal energy is the most important one of these resources with its tectonic conditions (Alacali, 2018). Erzurum is located away from 70 km of Karlıova Triple Junction (KTJ), where the North Anatolian Fault Zone (NAFZ) and the East Anatolian Fault Zone (EAFZ) converge (McKenzie, 1976; Dewey et al., 1986; Le Pichon et al., 1995; McClusky et al., 2000). The EAFZ, almost in the northeast direction, shows strike-slip fault mechanisms (Bulut et al., 2012). This fault zone is a transform fault and forms between the Anatolian and the Eurasian plates and between the Arabian and African plates (Westeway, 1994). It extends from Karlıova in the northeast to Kahramanmaraş in the southwest and is thought of as a conjugate structure to the NAFZ (Bozkurt, 2001). The EAFZ consists of six main segments, approximately 550 km long, and is the second-largest tectonic unit in the micro-Anatolian plate (McKenzie, 1976; Duman and Emre 2013). The EAFZ is located in the southwest of the KTJ where these two mega faults converge (Italiano et al., 2013; Simao et al., 2016). The NAFZ is the largest tectonic unit in the micro-Anatolian plate, with a length of about 1500 km (Ketin, 1976). These transform fault zones are one of the most seismically and tectonically active regions (Bozkurt, 2001) and forms between Eurasian plate to the north and the Anatolian plate to the south (Figure 1). It extends from the Saros Gulf in the northern Aegean Sea to Karlıova in the eastern Turkey (Şengör et al., 2004). The NAFZ is also characterized by several second order faults and the dextral shear related to the NAFZ proceeds across the northern Aegean (Bozkurt, 2001). Dextral motion along the NAFZ is about 24–30 mm/year (Reilinger et al.,

* Correspondence: eren.pamuk@mta.gov.tr

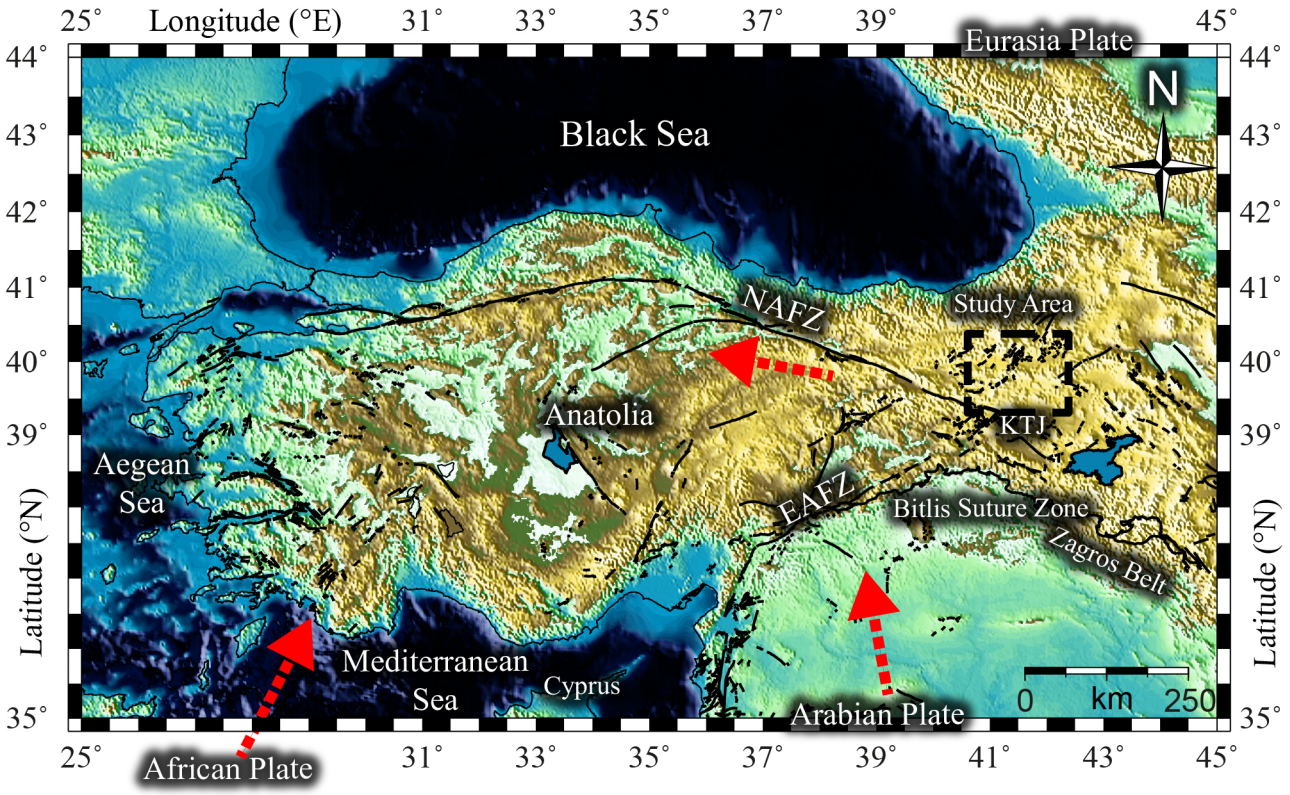

Figure 1. The general tectonic structure and general morphology of the Anatolian block. Abbreviation: NAFZ: North Anatolian Fault Zone, EAFZ: East Anatolian Fault Zone, KTJ: Karlıova Triple Junction. The black dashed line indicates the study area. The red arrow shows the representative plate motions. The thin black lines represent the tectonic unit of the Anatolian block from Emre et al. (2013; 2018). Arrows show GPS velocity direction in Anatolia relative to Eurasia (Reilinger et al. 1997; Le Pichon and Kreemer, 2010; Dilek and Sandvol, 2015).

1997). The region to the east of the KTJ is defined by a north-south compressional tectonic structure. The area is dominated by conjugate strike-slip faults of dextral and sinistral features paralleling the NAFZ and EAFZ (Bozkurt, 2001). The conjugate strike-slip fault system controls the active tectonics of the eastern Anatolia. However, the east-west trending basins of compressional origin form the most spectacular structures of the region (Wong et al., 1978).

Indeed, seismic *b* - value is one of the most significant seismo-tectonic parameters related to the material heterogeneity, thermal characteristics, and strength of the rocks for a given region (Wiemer et al., 1998; Maden and Öztürk, 2015; Öztürk and Sahin, 2019). However, the correlations among the *b* - value, gravity and magnetic anomaly, heat flow, Curie point depth (CPD), tilt angle and total horizontal derivative, P-wave velocity (Vp) change and Vp / Vs (P-wave velocity / S-wave velocity) ratio have not been researched in detail for different parts of the world. The *b* - value is a scaling law of earthquake distributions, and literature studies indicate that *b* - value is not only related to the relative proportion of the small and great events but it also reflects the properties of the seismogenic environments, regional-temporal-depth variations of stress, rheological and geotectonic properties of the Earth's materials (Ogata et al., 1991; El-Bohoty et al., 2012; Kalyoncuoglu et al., 2013; Abdelfattah et al., 2020). Deviations from the average *b* - value (~ 1) may be due to different reasons. If there is an increase in material heterogeneity or fracture density, large *b* - values can be observed (Mogi, 1962). However, a decrease in the confining pressure or an increase in the shear stress gives low *b* - value (Scholz, 1968). Cao and Gao (2002) stated that *b* - value can be related to the plate subduction rate and, hence, an increase in plate subduction rate may lead to an increase in volcanic activity. Although there may be a relation among *b* - value, gravity anomaly and heat flow data (Wang, 1988), there does not exist enough studies explaining the relations among these types of parameters for different parts of Turkey.

Curie depth is known as the temperature at which the magnetization disappears. The CPD values are often used in determining the thermal structure of the crust and estimating potential geothermal areas. The EMAG2

(The global Earth Magnetic Anomaly Grid 2) magnetic data set has been widely used in research in recent years to calculate the CPD values. Li et al., (2017) used EMAG2 magnetic data set to obtain the first global model of CPD. Njeudjang et al. (2020) used EMAG2 data to determine CPD, heat flow, and geothermal gradient values for the Adamawa volcanic region. Pamuk (2019) estimated CPD, surface heat flow values, and boundaries of buried geological structures using the EMAG2 magnetic data for the northern part of the EAR of Turkey. Xu et al. (2017) estimated the top of the magnetic layer and CPD values using the EMAG2 data set for North China. Idarraga-García and Vargas (2018) determined the depth to the bottom of the magnetic layer in South America using the inversion of the EMAG2 magnetic anomaly data.

The local earthquake tomography (LET) method has been widely applied to investigate the upper crustal structure, volcanic areas, tectonic units, and geothermal areas. In its most basic form, the Vp provides lithological information, and the Vp / Vs ratio can be associated with petrological findings (Hauksson, 2000; Kaypak, 2008; Kaypak and Gokkaya, 2012). It can be concluded that geothermal systems are transported from a heat source by interpreting Vp and Vp / Vs models, including the LET method (Hauksson, 2000; Kaypak and Gokkaya, 2012; Ozer and Polat, 2017). Ozer and Ozyazicioglu (2019) reported the seismic velocity structure of Erzurum using ten years of data from 2007 to 2017. We used a new earthquake catalogue recorded between 2018 and 2020 for LET analysis in this study. Additionally, the time-dependent variation of four-dimensional tomographic changes can be traced with additional synthetic testing through this study.

Keskin et al. (2006) explained the evolution of collision-related volcanism, which may have an important role in geothermal studies with the help of the magma plumping model for the Erzurum - Kars Plateau. Bektas et al. (2007) reported that Curie point depths (CPD) ranged from 12.9 km to 22.6 km in the EAR using aeromagnetic, heat flow, and gravity data. Oruç et al. (2013) drew attention to the oil potential of Erzurum estimating the basement undulation from the inversion of Bouguer anomalies. Maden et al. (2015) stated that the thickness of sediment was ~5 km and the depth of Conrad and Moho ranged between 22 and 26 km and 41.0 and 44.5 km, respectively in Erzurum and its surroundings. Koçyiğit and Canoğlu (2017) emphasized that geothermal fields were not studied well enough in Erzurum pull-apart basin. Kaygusuz et al. (2018) described the evolutionary development of the Kandilli-Erzurum volcanic rocks with the help of geochemical data.

The tectonics of Erzurum and its surroundings has four main tectonic distinct. The tectonic lineaments are Erzurum-Dumlu left - lateral strike - slip fault (EDFZ), Palandöken Fault Zone (PFZ), which is consisted of left-lateral reverse-slip fault in the south, Aşkale left - lateral strike - slip fault (AFZ) in the North-Northwest, and Başköy-Kandilli Fault Zone (BKFZ) (Keskin et al., 2006; Kocyigit and Canoglu, 2017). Another importance of these tectonic units comes from their location around potential geothermal systems (Keskin et al., 2006). For this reason, it can be important to examine some properties of this area with different methods. In the scope of this study, a comprehensive analysis was achieved on the correlations between different parameters such as the b - value, magnetic anomaly, the CPD, tilt angle, and total horizontal derivative to detect edge detection of the geological structure, the Vp perturbation and the Vp / Vs ratio with different distances and depths in and around Erzurum. Thus, the results obtained by using the b - value, the Vp, the Vp / Vs, the CPD, and edge detection can be analysed to map the tectonic and geothermal areas associated with tectonic framework. Hence, we aimed to better understand and identify the geodynamic implications in the study area.

2. Methods

2.1. Regional and temporal analyses of the seismic activity

The earthquake catalogue operated in the statistical calculations such as time-magnitude distribution of seismic activity, the magnitude of completeness and region-time distributions of b - value was supplied from Öztürk (2009) for the time interval between 1970 and 2006 (see Bayrak et al., (2009) for details). In order to compose a homogeneous and thorough earthquake catalogue, Bayrak et al. (2009) used several databases such as International Seismological Center (ISC), Boğaziçi University, Kandilli Observatory and Research Institute (KOERI), National Telemetric Earthquake Observatory Network (TURKNET), Incorporated Research Institutions for Seismology (IRIS), The Scientific and Technological Research Council of Turkey (TUBITAK) and Disaster and Emergency Management Authority (AFAD). This earthquake catalogue is homogeneous for duration magnitude, M_d, and includes 2457 earthquakes for the study area with a depth less than 70 km from 1970 to 2006. In addition, the earthquake database from 2006 to 2020 was taken from the KOERI and AFAD. In order to obtain a homogeneous catalogue for Md between 2006 and 2020, we used the empirical relationships between M_d and M_L (local magnitude) given by Bayrak et al. (2009) since KOERI and AFAD generally give M_L in recent years. In fact, the database used in this study was basically taken from KOERI. However, fewer events may be missed in the KOERI catalog, and, thus, these

earthquakes were compiled from the other catalogs. The part of the earthquake database on the KOERI until 2012 shows that given magnitude type is M_d, but after 2012, it is gradually started to transform to M_L. Therefore, instead of converting a 40 - year M_d type to the last 8 - year M_L. type, it has been deemed more appropriate to use the data for the last 8 years of empirical M_d - M_L relations. In this way, the errors in the magnitude conversions were further reduced. For this reason, M_d type was used instead of the other magnitude types for more reliable results and magnitudes in the target catalog were not calculated empirically. Although the empirical relationship is not specific to the field of the study area, it includes the regions 1 and 24 in Bayrak et al. (2009), and these two regions cover Erzurum and its surroundings. 6276 earthquakes with $M_d \geq 1.0$ for the study area were acquired in the time interval between 2006 and 2020. The shallow events with depths less than 70 km were used to evaluate parameters because the seismogenic layer thickness is specified to 40–50 km for the Eastern part of Turkey including the study area (Gok et al., 2007). As a result, a catalogue consisting of 8733 shallow earthquakes (depth < 70 km) from April 21, 1970 to December 31, 2019, about 49.69 years, having a magnitude interval between 1.0 and 6.4 was obtained. The epicenter distributions of all events and the strong mainshocks with $M_d \geq 5.0$ were shown in Figure 2.

Gutenberg–Richter (1944) defines the empirical relation between the magnitude and a cumulative number of earthquakes by the following equation:

$$\log_{10} N(M) = a - bM \quad (1)$$

where N(M) is the cumulative number of earthquakes during a certain time spacing with magnitudes equal to or larger than M. One of the most important tools in the earthquake statistic is the Gutenberg–Richter (G–R) relation. This law is supposed to be the statement of earthquake self-similarity. The logarithmic relation between the magnitude and cumulative number of earthquakes assumes a power - law distribution for earthquake energy. Also, estimation of the *b* - value is significant for evaluation of the earthquake recurrence time and occurrence probability. *b* - value estimation shows a fractal relation between earthquake occurrence and the radiated energy, seismic moment, or fault length (Frohlich and Davis, 1993). The *a* - and *b* - values are positive constants: the slope of the magnitude-frequency distribution gives *b* - value; however, *a*-value is related to the earthquake activity level. *a* - value shows significant changes for different regions and these variations depend on the length of the study region, time period of the catalogue as well as the number of events (Öztürk, 2018). Utsu (1971) stated that the *b* - value changes between 0.3 and 2.0 in different seismic parts of the world. However, the calculated *b* - value ranges from 0.6 to 1.4 (Wiemer and Katsumata, 1999) and an average of *b* - value in the G - R relation equals approximately 1.0 (Frohlich and Davis, 1993). Although the *b* - value is associated with the relative proportion of small and large events, many factors can affect the changes of the *b* - value. The *b* - value has been used to evaluate the earthquake activity in terms of a large scale of magnitude scales based on the tectonic structures, anisotropic environments, and stress heterogeneities. Laboratory studies suggest that a tendency to decrease in *b* - value is related to an increase in shear stress and a reduction in restricted compression (Scholz, 1968). Also, crack density, thermal gradient, geological complexity, fault length, material properties, seismic wave velocity changes and attenuation, slip distribution, and strain circumstances lead to changes in *b* - value (Mogi, 1962; Scholz, 1968; Ogata et al., 1991; Schorlemmer et al., 2005; Ansari, 2016). In magmatic zones, earthquake activity is described with large *b* - values, hence, it means small effective stress relaxation that is related to high pore pressures and geothermal gradients (Abdelfattah et al., 2020). Thus, the *b* - value is the important coefficient for rheological-geotechnical features (De´verche`re et al., 2001; Fagereng, 2001; Kalyoncu et al., 2013; Maden and Öztürk, 2015).

The usage of the maximum number of earthquakes is crucial and essential for superior quality results for the evaluation of region – time - magnitude changes of the seismicity, in the analysis of magnitude-frequency distribution. As the first step, the minimum magnitude of completeness, Mcomp, formed on the conjecture of Gutenberg - Richter scaling - size distribution of magnitudes is able to be calculated. Mcomp can be theoretically defined as the smallest magnitude that all the events are analyzed (Habermann, 1983; Mignan and Woessner, 2012). This means that Mcomp levels include 90 % of the earthquakes being sampled with a power-law fit (Wiemer and Wyss, 2000; Öztürk and Sahin, 2019). Mcomp changes with space and time and hence, time analysis of Mcomp may produce wrong estimates of seismotectonic parameters, especially *b* - value. In order to observe the temporal changes of Mcomp, a moving time window approach is generally used and temporal changes of Mcomp can be estimated. Thus, the knowledge of temporal Mcomp is very important, and the estimation of Mcomp time variations was achieved carefully as the first step in this detailed statistical.

2.2. Local earthquake tomography (LET)

Station coordinates and arrival times of P- and S- seismic rays from local earthquakes constitute primary data for LOcal TOmography Software (LOTOS). Earthquake parameters (epicenter, focal depth, origin time) are relocated simultaneously using location of events and

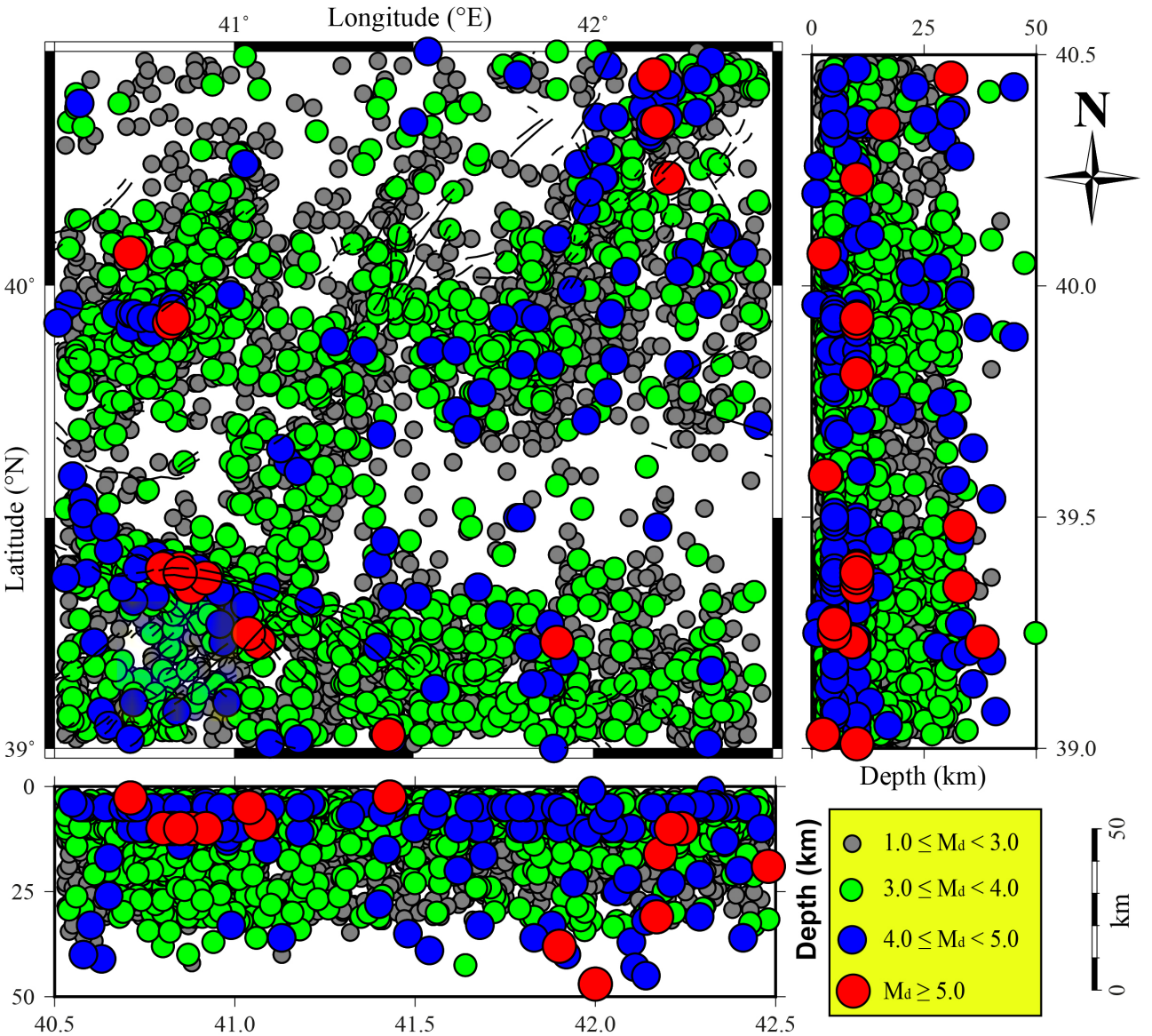

Figure 2. Epicenter distributions of earthquakes recorded between 1970 and 2020 in and around the Erzurum region. The black lines show tectonic units of the study area (Emre et al., 2013; 2018).

one-dimensional (1 - D) velocity structure to obtain three-dimensional (3 - D) velocity structure. Earthquake source location is defined using goal function (GF) which expresses the possibility of the source location at 3 - D space (Koulakov, 2009). The process of estimating the earthquake parameters by inverting with some preliminary assumptions is a classic inversion process. Initial location results obtained by the Hypo71 (Lee and Lahr, 1975) algorithm are submitted as input to the LOTOS - 12 (Koulakov, 2009) program for the determination 3 - D seismic velocity structure in this study. The 3 - D tomographic calculations are performed using the earthquakes re-located with the LOTOS - 12 algorithm. The inversion coefficients such as smoothing factor are determined using synthetic tests. The LSQR method is utilized for the inversion of model matrix (Page and Saunders, 1982; Van der Sluis and Van der Vorst, 1987). Koulakov (2009) described in detail the mathematical foundations and use of the LOTOS - 12 algorithm.

Checkerboard testing is one of the most common synthetic tests to examine the accuracy of a 3 - D velocity tomography model. The character of the tomographic image is significantly affected by the model inversion parameters. In checkerboard testing, the inspection area is divided into rectangular prisms, and each of these prisms is assigned as high and low - velocity values, consecutively. In

the synthetic model, synthetic travel times are calculated, synthetic travel times are processed with tomography, and the validity of the original checkerboard-shaped velocity structure is examined. If the desired extent of the image could not be obtained by synthetic tests, the test is performed by changing the inversion parameters used in tomography. After an optimum model is obtained in these tests, the process is terminated to use these parameters in the real data (Ozer, 2019; Ozer and Ozyazicioglu, 2019). As a result of synthetic tests carried out in this study, it was determined that the tomographic images were reliable between 0 and 25 km (Figure 3).

2.3. EMAG2 magnetic data and edge detection analysis methods

The global Earth Magnetic Anomaly Grid 2 (EMAG2)" was used as total field magnetic anomaly data in this study. EMAG2 magnetic data include satellite, vessel, and air measurements (Maus et al., 2009). This global model is a spherical grid with a height of 4 km, a resolution of 2 arc - min (Maus et al., 2009).

It is important to image the boundaries of buried geological structures in making sense of potential field data such as gravity and magnetic. There are numerous methods of boundary analysis based on derivatives to determine the boundaries of geological structures. Some of these commonly used methods are total horizontal derivative (THDR) and tilt angle (TA). In this study, the source boundaries of the structures causing the magnetic anomaly were mapped by THDR and TA methods. The total horizontal derivative (THDR) proposed by Cordell and Grauch (1985) can be calculated using formula 2:

$$THDR = \sqrt{\left(\frac{\partial M}{\partial x}\right)^2 + \left(\frac{\partial M}{\partial y}\right)^2} \quad (2)$$

where M is the magnetic anomaly and ∂G / ∂X and ∂G / ∂y are the horizontal derivatives of the magnetic anomaly. TA can be found by calculating the ratio of the vertical derivative to the THDR (Miller and Singh, 1994):

$$\mathrm{TA} = tan^{-1}\left(\frac{\frac{dM}{dz}}{THDR}\right) \quad (3)$$

where TA is tilt angle, ∂M / ∂z is the vertical derivative of the magnetic anomaly, THDR is the total horizontal derivative.

2.4. Curie point depth

CPD values were computed using the technique proposed by Okuba et al. (1985) and described below. In Okuba et al. (1985) method, z_0 is the depth of the centre of the structure in formula 4, zt is the top depth of the structure in formula 5. In order to calculate Curie point depth (z_b, CPD), z_0 and z_t must be calculated correctly and reliably. In the first, the central depth of the source causing the magnetic anomaly is computed z_0 using formula 4:

$$In\left[\frac{P(s)^{1/2}}{|s|}\right] = InA - 2\pi|s|z_0 \quad (4)$$

z0 is the central depth of the source causing the magnetic anomaly, P (s) is the radially averaged power spectrum of the magnetic anomaly, A is the constant, and |s| is the wavenumber. In the second phase of the study, top depth of the structure (z_t) causing magnetic anomaly was calculated in the second method of Okubo et al. (1985) (formula 5):

$$n\left[P(s)^{1/2}\right] = InB - 2\pi|s|z_t \quad (5)$$

where B is a sum of constants which is independent of the wavenumber |s|. The depth to the top boundary z_t was acquired from the slope of the second-longest wavelength of the spectral segment of the second spectrum. After calculating z_t and z_0, z_b (CPD) can be easily calculated with the help of Eq. (6):

$$b = 2z_0 - z_t \quad (6)$$

The magnetic anomaly map was divided into 16 different blocks with 60 km * 60 km cell to determine CPD values (Figure 4). All blocks coincided with adjacent blocks by 50 %. This means that the distance of the centers of the two blocks to each other is about 30 km. The center of the blocks is marked with a triangle sign and shown in Figure 4. The power spectrum method (Spector and Grant, 1970) was applied to each block. The steepest slope was used to calculate the z_t. To calculate z_0, the power spectrum is separated by " s " and plotted against the wavenumber (Pamuk, 2019).

3. Results

3.1. Regional and temporal analyses of the seismic activity

The number of earthquakes in cumulative form as a function of time was presented in Figure 5. This form includes the original catalogue with $M_d \geq 1.0$ covering 8733 events and the completed catalogue with $M_d \geq 2.7$ containing 5535 events. As seen in Figure 5, any significant variations do not exist in the number of events from 1970 to 1995. There is a little change in earthquake activity from 1995 to 2003, whereas there is a remarkable increase in seismicity after 2003. However, there exist significant increases in the number of earthquakes, especially starting after 2005. Time histogram of the earthquakes from 1970 to 2020 was plotted in Figure 6a and the increase in the number of events in 2003 can be seen clearly. Also, there exists a maximum increase in the number of earthquakes in 2015. Magnitude interval of the database changes between 1.0 and 6.4 with an exponential decay in the number from

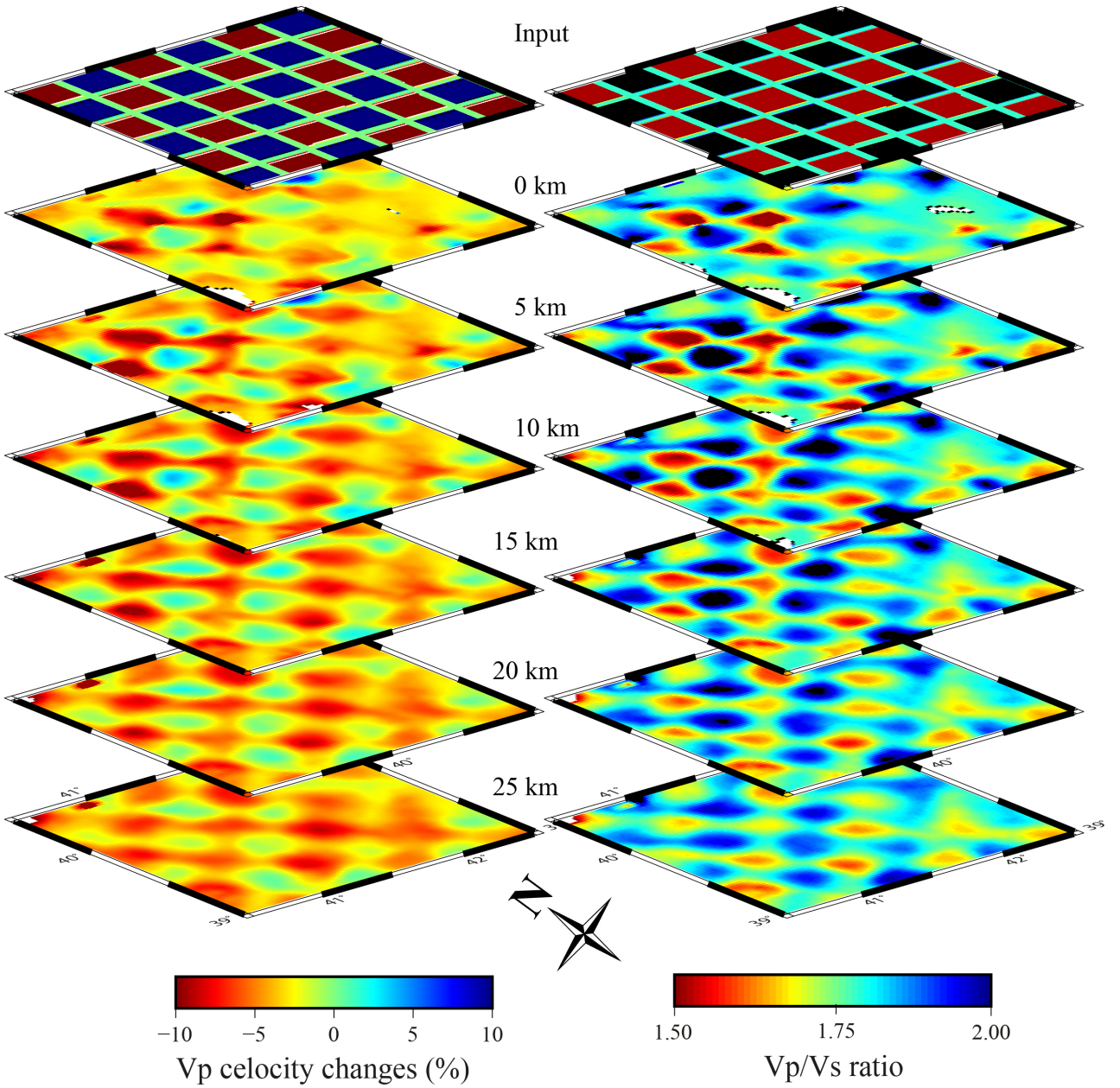

Figure 3. Checkerboard tests of the tomographic model.

smaller to larger levels. Magnitude histograms of the earthquakes were given in Figure 6b. As shown in Figure 6b, the magnitudes of several earthquakes change between 2.5 to 3.2 and a maximum was observed at M_d = 2.7 level.

Temporal variation of Mcomp was estimated by using a moving time window approach and plotted in Figure 7. Then, the Gutenberg-Richter *b* - value was calculated by considering this Mcomp value. Estimation of magnitude completeness was realized with the samples of 50 earthquakes/window by using all 8733 events with $M_d \geq$ 1.0. There exist rather large values of Mcomp from 4.0 to 4.5 between 1970 and 1997, whereas it shows a remarkable decrease to about 3.0 at the beginning of 2009. Then, it decreases to about 2.8 at the beginning of 2012 and has relatively small values changing between 2.4 and 2.8 for the latest events after 2012. Although Mcomp generally has non-stable values in the different time intervals, it can be concluded that Mcomp = 2.7 can be acceptable, representing all the time period of the catalogue, which is consistent with the results of literature studies including this region such as Öztürk (2017; 2018). *b* - value of the Gutenberg-Richter relation for all earthquakes was shown

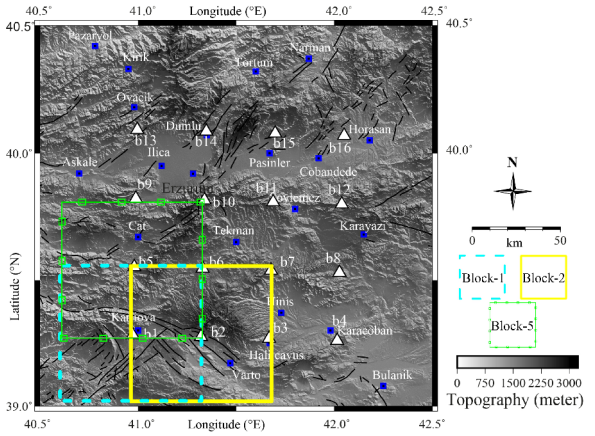

Figure 4. The blocks used in CPD analysis. The squares indicate three blocks (B1, B2, and B5). Block sizes are 60 × 60 km^2. The triangles symbol shows the blocks' centres and numbers utilized for the CPD regions. The black lines show tectonic units of the study area (Emre et al., 2013; 2018).

in Figure 8. For the estimation of the *b* - value, the maximum likelihood method was used since this method yields a more robust estimate than the least-squares regression method (Aki 1965). Using the frequency-magnitude distribution of earthquakes and considering Mcomp = 2.7, the *b* - value was computed as 1.06 ± 0.06. As stated above, the earthquakes are represented by a *b* - value from 0.3 to 2.0 and more frequently around 1.0 with an average. It can be concluded that the magnitude-frequency distribution of the earthquake occurrences is well represented by the G - R relation with the *b* - value typically close to 1 (Figure 8).

In order to describe the different characteristics of *b* - value in the specific zones, b - value variations with depth were analysed and illustrated in Figure 9. These changes were also given in detail in Table 1. As seen in Figure 9 and Table 1, detailed b - value maps from the surface to a depth of 60 km were achieved for every depth interval of 5 km. An overlapping depth of 5 km (moving step) was considered to provide continuity of the data. Figure 9 shows that there exist significant fluctuations between 0 and 35 km and *b* - values have a relatively decreasing tendency in these depths, changing from 0.65 to 1.29. However, a clear increase in *b* - value (from 0.87 to 1.04) was observed in 20 km. A sharp increase from 0.65 to 1.45 was observed between 35 and 40 km depths. Large *b* - values related to depth, associated with the lower crust, show that the study region can be explained with a strong lithosphere (Khan and Chakraborty, 2007). The larger *b* - values may be affected by magma chambers and following normal stress decreases (Sanchez et al., 2004). On the contrary, although there exists a small increase in *b* - value (from 1.03 to 1.14) between 45 and 50 km, a strong decrease from 1.45 to 0.91 was also observed after this depth range (depth > 40 km).

In addition to averaged *b* - values for every 5 km depth interval, regional changes of *b* - value were also plotted in these depth ranges and shown in Figure 10. The *b* - value was estimated by using a moving window approach with

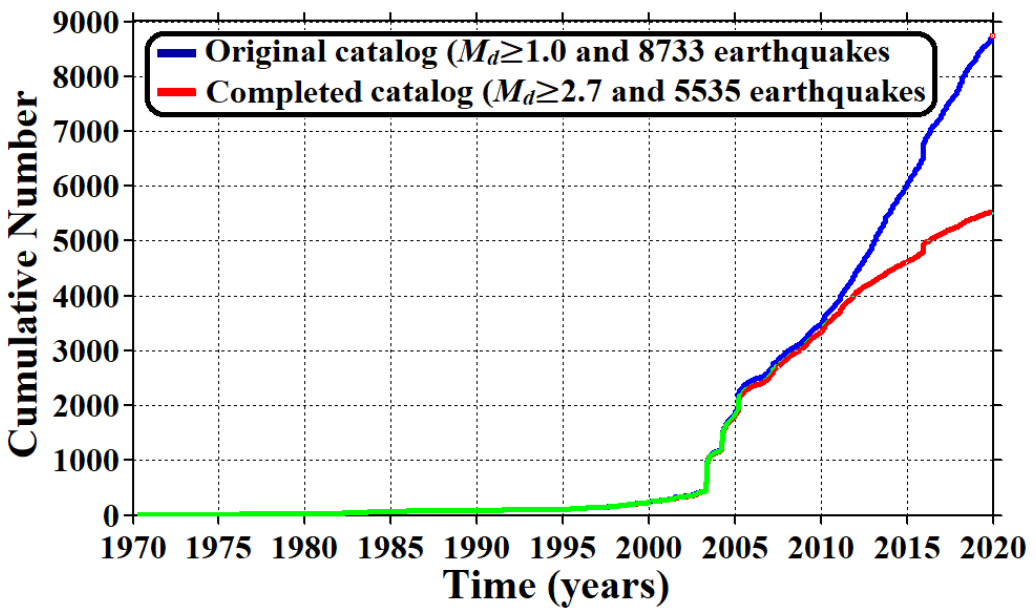

Figure 5. The cumulative number of events as a function of time from 1970 to 2019 in and around Erzurum. Blue line shows the original catalogue including all 8733 earthquakes and the red line indicates a completed catalogue including 5535 events.

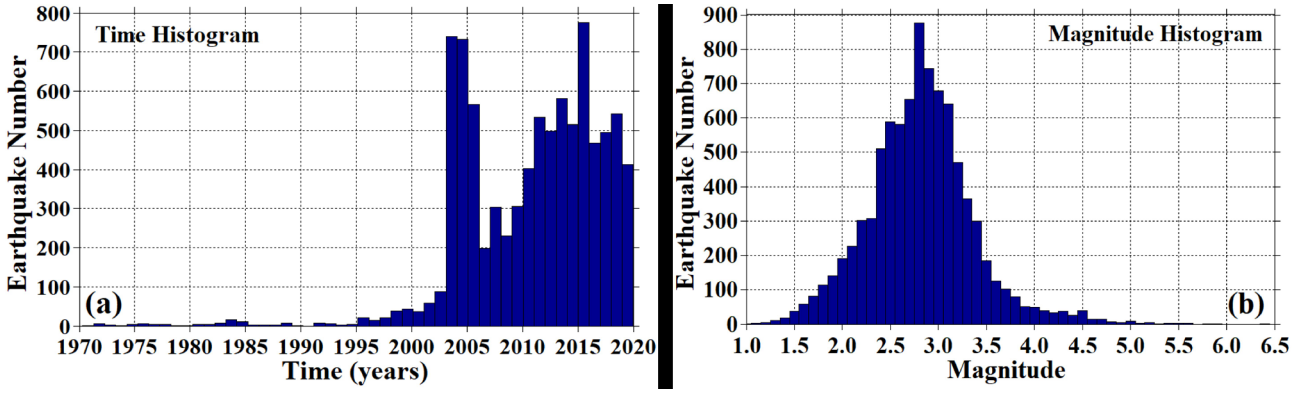

Figure 6. (a) Time (b) Magnitude histograms of the earthquakes between 1970 and 2020 in and around Erzurum.

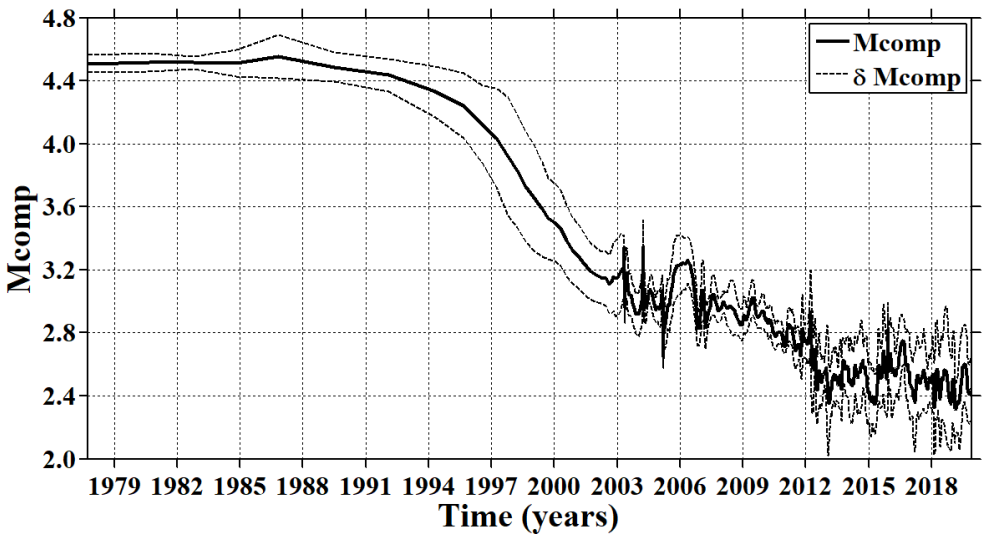

Figure 7. The magnitude of completeness, Mcomp, as a function of time between 1970 and 2020. The standard deviation (δMcomp) of the completeness (dashed lines) was also plotted.

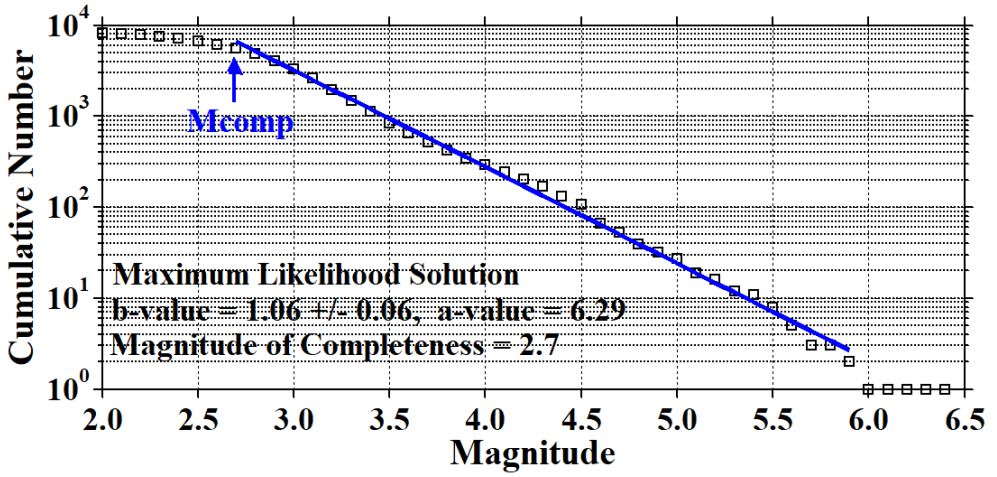

Figure 8. *b* - value of Gutenberg-Richter relation. The standard deviation of *b* - value, Mcomp and a-value was also given.

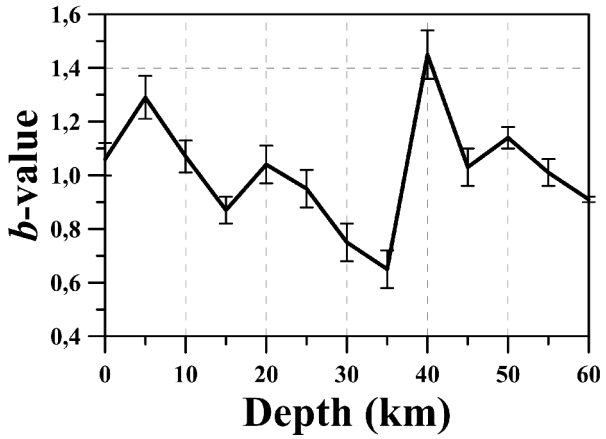

Figure 9. *b* - value changes with depth.

the maximum curvature method (MAXC) described in Woessner and Wiemer (2005). In order to calculate the *b* - values, the different number of earthquakes, different sample sizes, different magnitude intervals, and different Mcomp values were used concerning the earthquake occurrences in different depths. A regional grid of points with a space of 0.03º in longitude and latitude was used. As shown in Figure 10, *b* - values generally show a strong increasing and decreasing trend (from 0.5 to 2.0) in the same regions for depths of 0 and 5 km. Maden and Öztürk (2015) pointed out that *b* - values vary between 1.2 and 1.5 in Aşkale and Erzurum faults and that these values are high. Öztürk (2018) suggested that *b* - values are smaller than 1.0 and indicated an earthquake potential in the EAR. The largest *b* - values (> 1.75) were observed among Aşkale, Ilıca, Dumlu, and Kırık in this study. The possible reason for this high *b* - value may be the release of magmatic gases caused by the pressure reduction at shallow depths. Groundwater interaction and the consequent normal stress reduction may also influence these larger *b* - values (Sanchez et al., 2004). Moderate *b* - values (1.0–1.5) for depths of 0–5 km were calculated in some areas such as Karaçoban, Tekman, Çat, and Karlıova. The other regions including Pasinler, Söylemez, Karayazı, Horosan and Narman have relatively small *b* - values (< 1.0). These types of similarities were also observed for depths of 10 - 15 km. However, *b* - values show a clear decreasing (< 0.75) in and around Karayazı and Karaçoban in 15 km. The areas with high and low *b* - values are the same for the depths of 20 and 25 km. For these depth ranges, *b* - values greater than 1.0 include Karlıova, Karaçoban, Tekman, Söylemez, Çat, Dumlu, Ilıca, Aşkale and Kırık, whereas *b* - values smaller than 1.0 include Karayazı, Pasinler, Narman, and Horosan.

3.2. Local earthquake tomography

The tomographic structure of the study area was investigated with the help of horizontal profiles using the initial 887 events recorded by more than sixty seismic stations with an RMS value of less than 0.50 were used. The well-located 594 earthquakes (total of 5054 P - and 3712 S - phases) recorded by the Disaster and Emergency Management (AFAD) and Atatürk University Earthquake Research Center weak ground motion stations from 2018 to 2020 were used (Figure 11a). The minimal number of

Table 1. Details of analysis for the earthquake occurrences in different depths. NOAE: Number of all events, NOEBC: Number of events in the *b - value* calculation, MIOAE: Magnitude interval of all events, MIOEBC: Magnitude interval of events in the *b - value* calculation, POEBC: Percentage of events in the *b - value* calculation.

Depth (km)	NOAE	NOEBC	MIOAE	MIOEBC	Mcomp	*b - value*	*a*- value	POEBC (%)
0	8733	5534	1.0–6.4	2.7–5.9	2.7	1.06 ± 0.06	6.29	63.37
5	5275	3024	1.0–5.5	2.8–5.5	2.8	1.29 ± 0.08	6.32	57.33
10	5895	3866	1.0–6.4	2.7–5.9	2.7	1.07 ± 0.06	6.13	65.58
15	2422	1231	1.1–6.4	2.8–6.0	2.8	0.87 ± 0.05	5.64	50.83
20	1094	508	1.3–5.8	2.7–4.9	2.7	1.04 ± 0.07	6.13	46.44
25	805	414	1.3–5.0	2.7–4.9	2.7	0.95 ± 0.07	5.99	51.43
30	555	348	1.3–5.6	2.7–5.5	2.7	0.75 ± 0.07	5.28	62.70
35	189	136	1.4–5.6	2.8–5.4	2.8	0.65 ± 0.07	3.99	71.96
40	31	12	1.1–5.1	4.4–5.0	4.4	1.45 ± 0.09	11.40	38.71
45	21	5	1.1–5.0	4.3–4.9	4.3	1.03 ± 0.07	7.98	23.81
50	15	7	1.7–5.0	4.3–5.0	4.3	1.14 ± 0.04	7.46	46.67
55	10	5	2.4–4.7	4.0–4.6	4.0	1.01 ± 0.05	1.74	50.00
60	15	6	2.4–4.7	4.2–4.7	4.2	0.91 ± 0.01	1.82	40.00

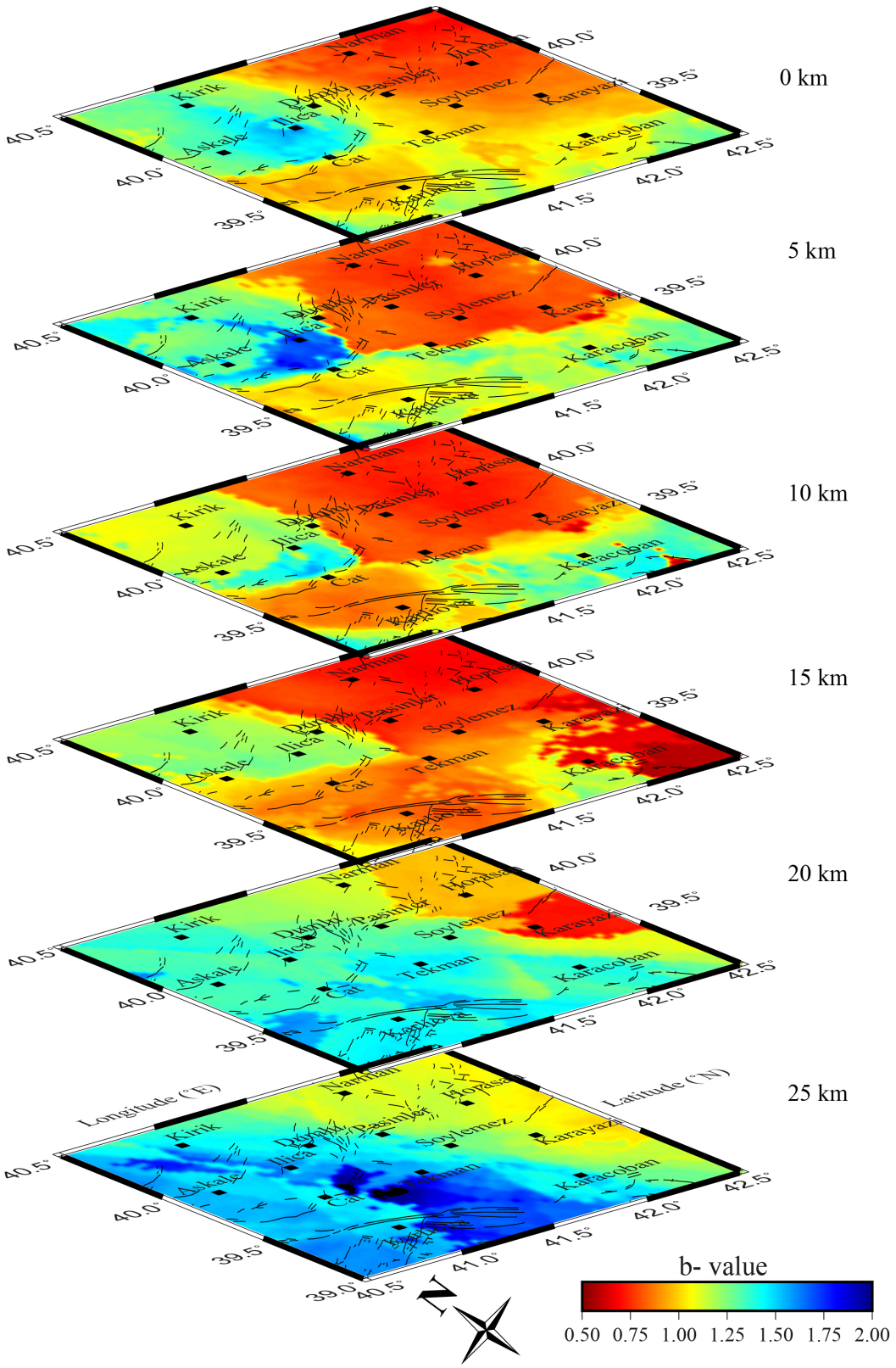

Figure 10. Regional changes of *b* - value for different depths such as 0, 5, 10, 15, 20, and 25 km. *b* - values at different depths were calculated by using a moving window approach with different input values as stated in the text. For the regional images, the cells spaced 0.03º in longitude and latitude were considered. The black lines show tectonic units of the study area (Emre et al., 2013; 2018).

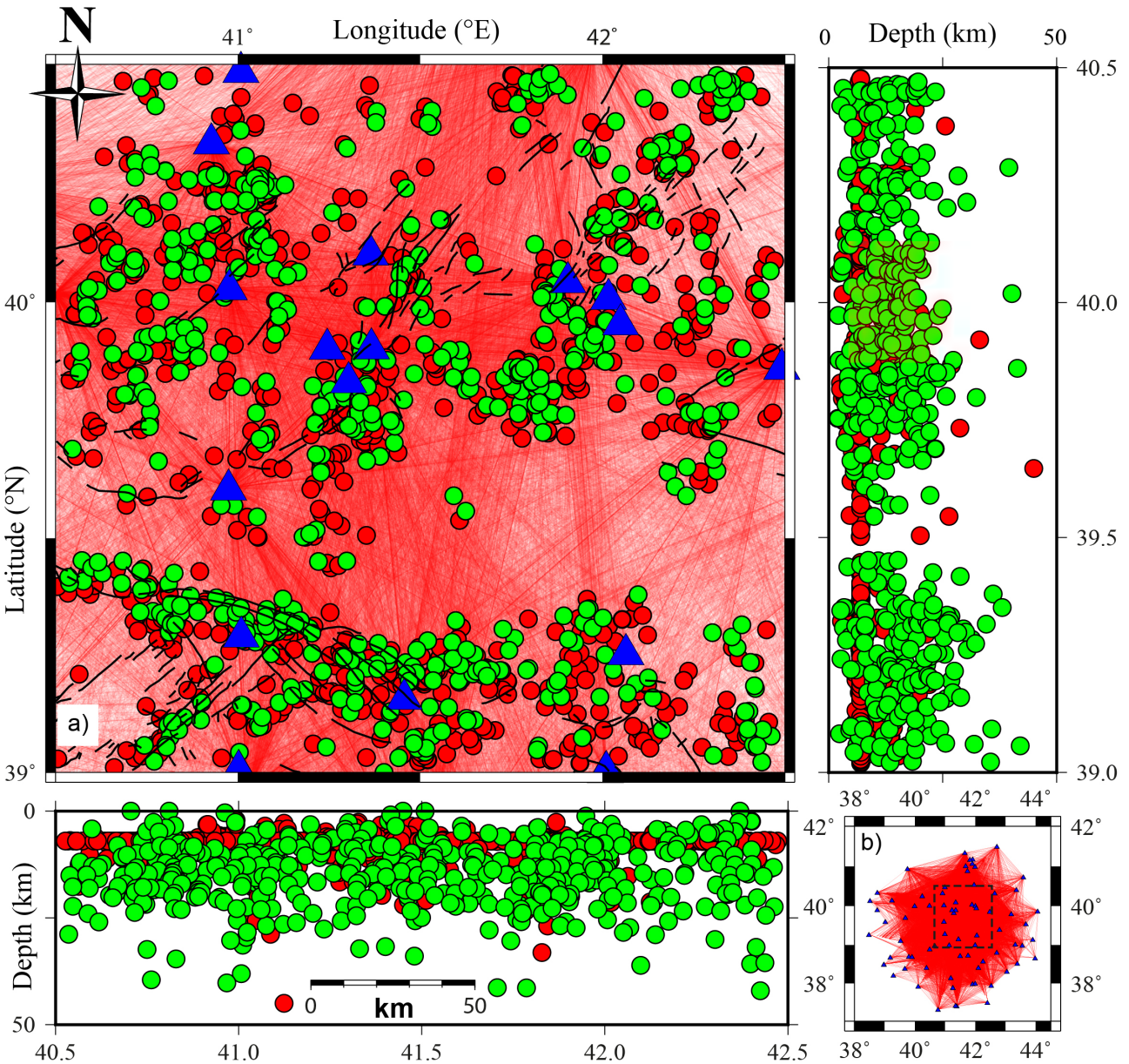

Figure 11. a. Location of initial 887 (red circles) and selected 594 (green circles) high-quality events recorded from 2018 to 2020 in the study area for the LET analyses. The black lines show tectonic units of the study area (Emre et al., 2013; 2018). The thin red line indicates ray path between station (blue triangle) and selected earthquake. b. Distribution of all stations and ray paths utilized in this study. The dashed black rectangle shows the coordinate boundaries converged in Fig. 11a at the same time that the findings were produced.

records is designed to be at least seven within the scope of the selection criteria. The 1 - D seismic velocity structure proposed by Maden (2012) is used to calculate the 3 - D tomographic calculations. It is also seen that the ray paths of the selected earthquakes cover the study area (Figure 11b).

In Vp and Vp / Vs models, horizontal profiles are designed with 5 km gaps between 0 - 25 km. The velocity changes in the horizontal profiles contain important information about the tectonic state of the region. The low-velocity areas increase as moving from the surface to the deep. This effect was observed clearly, especially in the 25 km horizontal slice. Especially in Karlıova and its surroundings (KTJ), the low velocities are noted in 0 and 5 km slices. This area is extremely active tectonically and 5.7 and 5.6 (Mw) magnitude earthquakes have occurred respectively on June 14 and June 15, 2020. More than 250 aftershocks occurred within one week after these

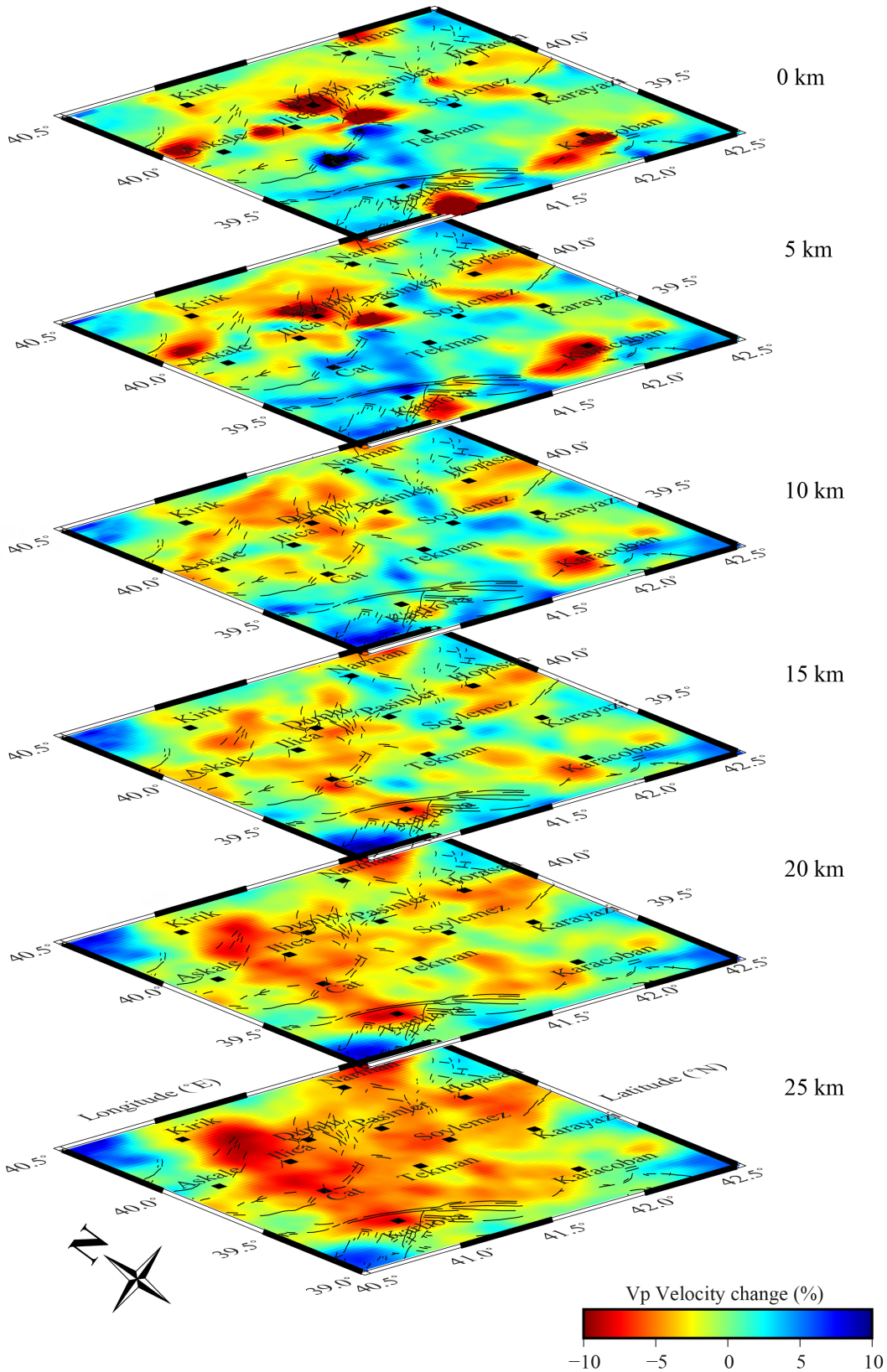

Figure 12. The Vp velocity perturbation of the horizontal section results from 0 to 25 km. The black lines show tectonic units of the study area (Emre et al., 2013; 2018).

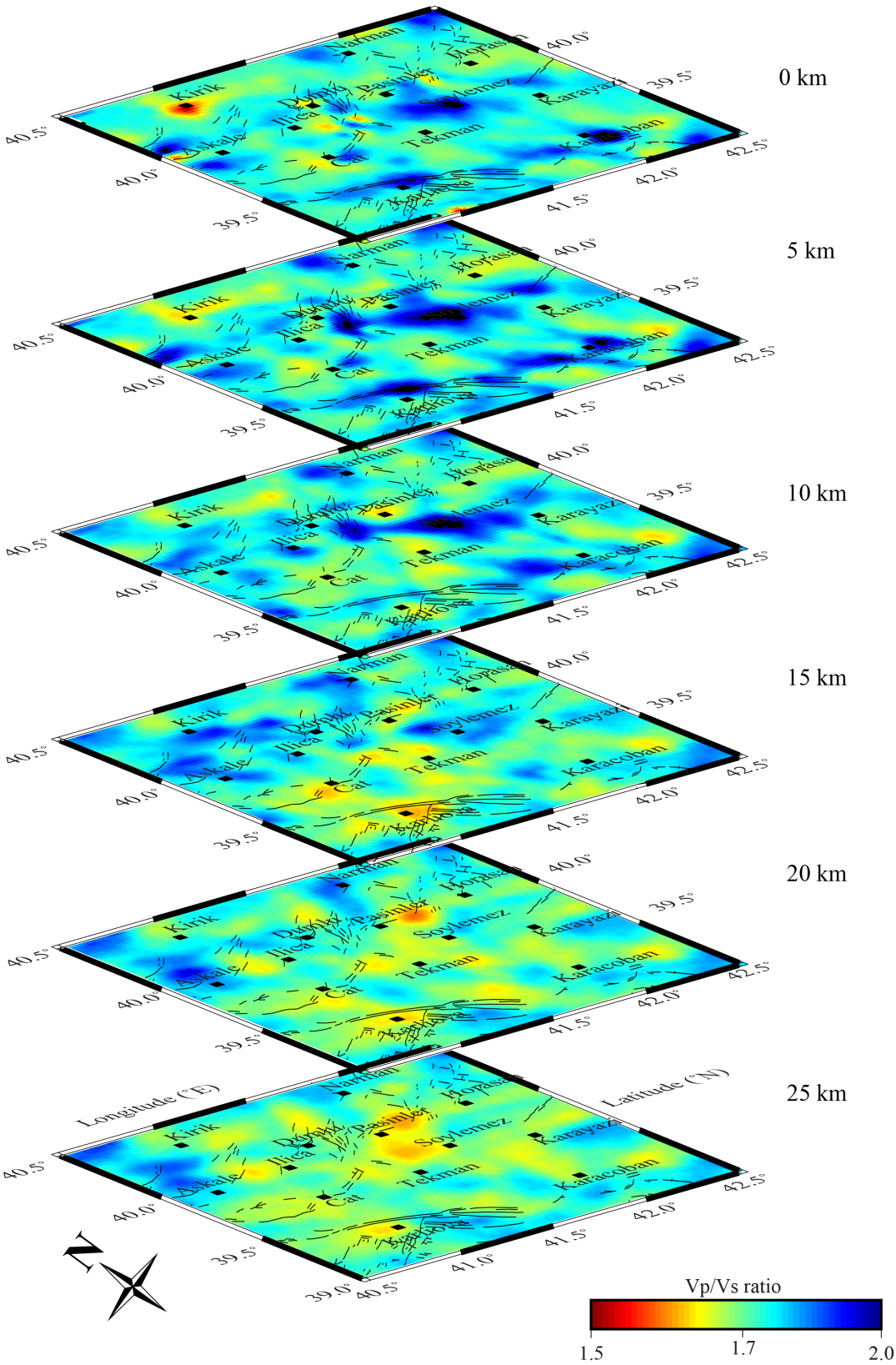

Figure 13. The Vp / Vs ratio of the horizontal section results from 0 to 25 km. The black lines show tectonic units of the study area (Emre et al., 2013; 2018).

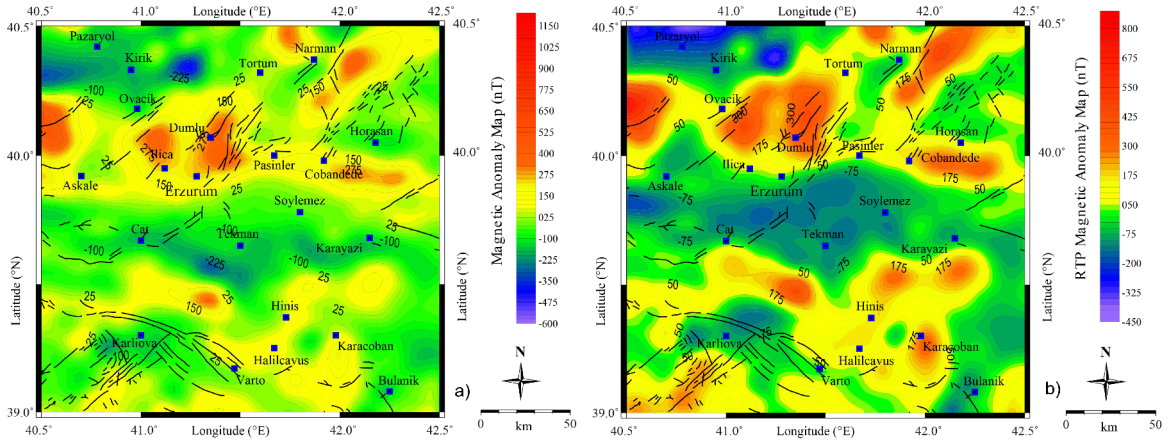

Figure 14. a) EMAG2 total field magnetic anomaly map (compiled from Maus et al. (2009)) b) RTP total magnetic anomaly map with major tectonic structures. The black lines show tectonic units of the study area (Emre et al., 2013; 2018).

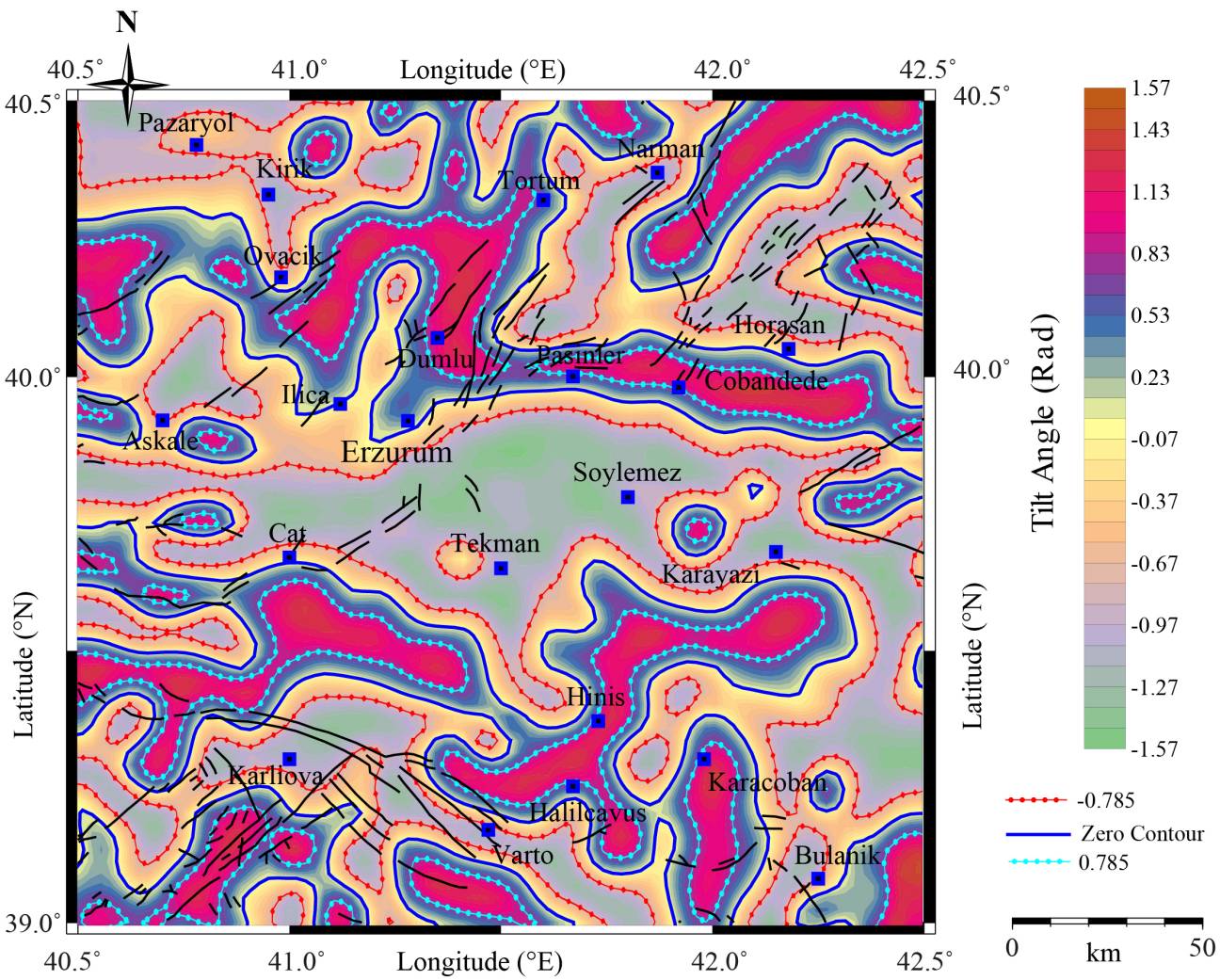

Figure 15. Tilt Angle (TA) map of RTP total field magnetic anomaly map. The black lines show tectonic units of the study area (Emre et al., 2013; 2018).

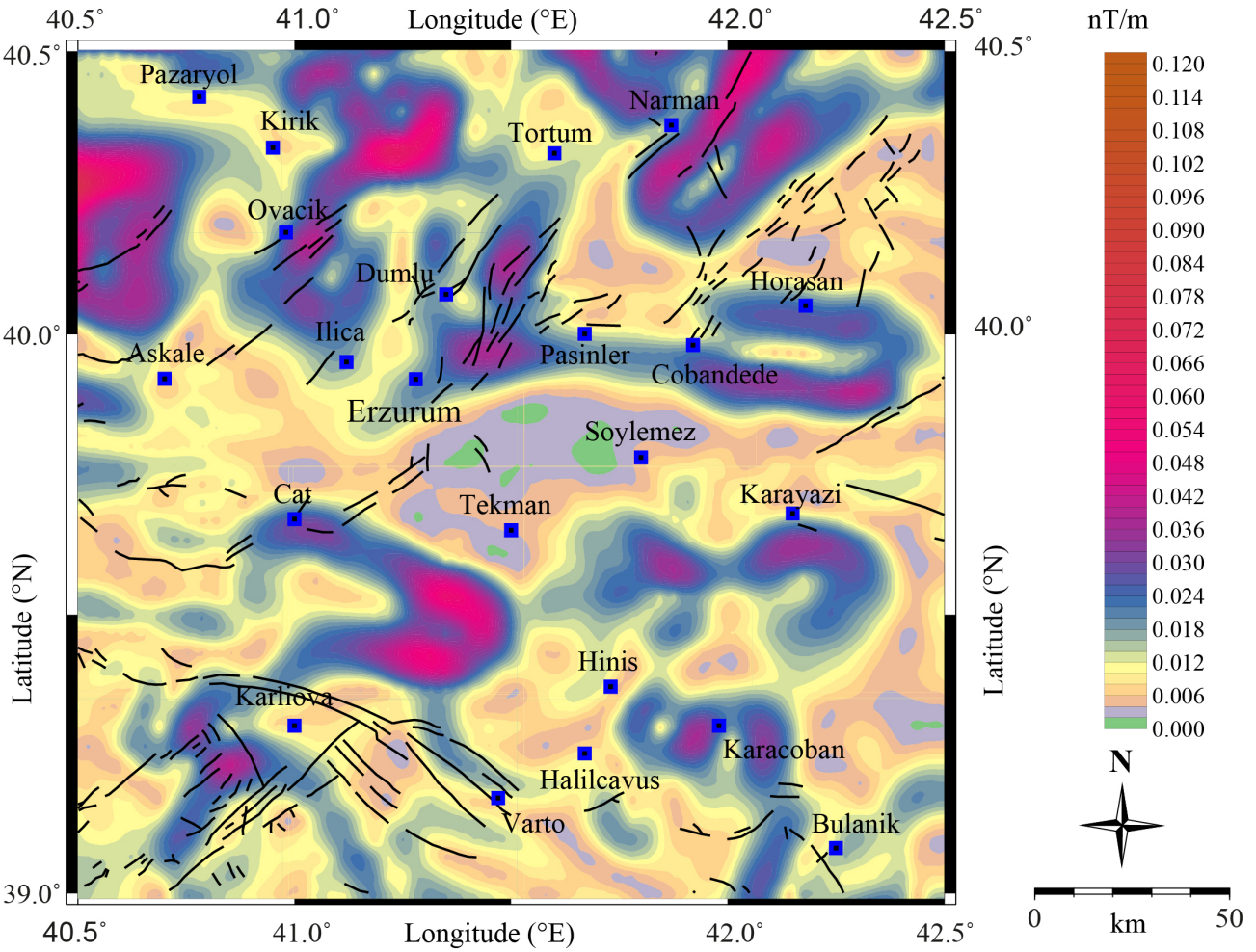

Figure 16. Total horizontal derivative (THDR) map of RTP total field magnetic anomaly map. The maximum amplitude values in the total horizontal derivative (THDR) map show source edges according to Cordell and Grauch (1985). The black lines show tectonic units of the study area (Emre et al., 2013; 2018).

earthquakes. Furthermore, the KTJ region has also been the scene of many destructive earthquakes throughout history. Another significant decline in velocity values has been observed around Karaçoban. The low velocities in this area are more effective between 0 and10 km and gradually decrease from 10 km through deep. The low velocities in Aşkale and Dumlu are noteworthy at 0 and 5 km. Aşkale and Dumlu are located in the area that contains the most important tectonic units within the study area (Figure 12).

In potential geothermal regions, where the Vp values and the Vp / Vs ratio are low may indicate CO2, gas, or a mixture of these. Moreover, there are some opinions that the combination of low Vp and high Vp / Vs might occur with geothermal fluids in the region (Hauksson, 2000; Kaypak and Gokkaya, 2012). Low Vp and low Vp / Vs, which may indicate the existence of geothermal systems, and especially low Vp and high Vp / Vs values were studied between 0 and 5 km. These depths include combinations of low Vp and high Vp / Vs in Aşkale, Ilıca, Dumlu, Pasinler, and Karaçoban from the west to the east. The most emphatic anomaly of these anomalies is in the Karaçoban region. This combination is very evident in 0 and 5 km horizontal slices for Karaçoban and gradually decreases with depth. Also, a combination of low Vp and Vp / Vs values was also detected in the Kırık region. For the exploration of the geothermal capacity of Kırık, it has great importance to be studied with other methods such as MT. (Figures 12 and 13).

3.3. Edge detection in magnetic data

In this study, a differential reduction to pole (RTP) method developed by Arkani-Hamed (1988, 2007) was performed on magnetic anomaly map (Figure 14a) to correct bipolarity phenomena of the magnetic data. The RTP magnetic anomaly map was examined, and it was observed that magnetic values ranged from - 450 nT to 800 nT (Figure 14b). Negative magnetic anomaly values (from 0

Table 2. Comparison of CPD values obtained from this study and previous studies (CPD values determined from previous studies were digitized from the maps of related studies).

Curie Point Depth (km)				
Block No	This study	Aydin et al. (2005)	Bektas et al. (2007)	Pamukcu et al. (2014)
b1	14.21	18	17.5	14
b2	15.49	20	18	14
b3	15.67	20	18	12
b4	14.90	18	18	12
b5	12.55	18	15	13
b6	15.64	18	16	12.5
b7	11.73	16	17	13.5
b8	15.77	14	17	14
b9	14.32	22	15.5	13
b10	16.15	20	16	13
b11	13.85	18	16.5	14
b12	14.90	14	16.5	16
b13	18.67	24	16.5	16
b14	19.16	24	16	16
b15	14.54	24	16.5	16
b16	16.52	22	16.5	16

to - 450 nT) were obtained in the Pazaryolu region, located in the northwest of the study area, in the Erzurum Centre, Tekman, Söylemez, and Çat regions located in the central parts of the study area. Positive magnetic anomaly values (50–800 nT) were calculated in Dumlu located at the north of Erzurum, Çobandede located in the northeast, Hınıs, Karaçoban, and Karayazı regions located in the southeast. In general, positive anomalies are noticeable, except for areas with thick alluvial units (Figure 14b).

Tilt angle values range from - π/ 2 to +π / 2. The tilt angle value is zero at the boundary location of the source; it is negative outside the source (Oruç, 2011). Therefore, the zero contours on the tilt angle map correspond directly to the structure boundary. In addition, the source depth can be obtained the half distance between ± π / 4 contours of TA map (Oruç, 2011). or the distance between zero and + π / 4 or – π / 4 contour of TDR, respectively (Salem et al., 2007; Oruç, 2011). So, the TA method has a very important place in determining the direction of the geological structure. The boundaries obtained by the THDR method and the boundaries obtained by the TA method are compatible with each other. The tilt angle (TA) map of the study area was shown in Figure 15.

In the north of the study area, the approximate direction of the geological structure boundaries is NW - SW. In this area, the direction of the faults indicated by the black line and the directions of the boundaries obtained from TA is almost the same. Boundaries of the basin, surrounding Erzurum center, Tekman, Söylemez and Çat districts, and alluvial units is determined by TA. The direction of the basin boundaries is approximately NW-SE. The faults at the northwest of the study area are consistent with the zero contours on the TA map. The boundaries of structures in this area are SW - NE oriented (Figure 15). In the examination of THDR distribution, NE - SW directional boundaries around Narman; E - W directional boundaries extending from Erzurum to Çobandede; NE - SW directional structure boundaries in the Northwest of Erzurum were obtained (Figure 16).

3.4. Curie point depth (CPD)

The least - squares method was used to determine the line that best fits the data points, and slopes were obtained (Figure 17). The power spectrum of the magnetic anomaly belonging to block - 4 is shown in Figure 17. z0 is obtained from the slope of the longest wavelength part of the spectrum divided by radial frequency (Figure 17a). Then zt is estimated from the slope of the second - longest wavelength part of the spectrum (Figure 17b). z0 was calculated as 8.33 km and zt as 1.76 km for block b4. CPD was obtained as 14.90 km. Calculated CPD values are given in Table 2 and Figure 17. In Table 2, the results of previous studies in the study area were also given and compared with this study.

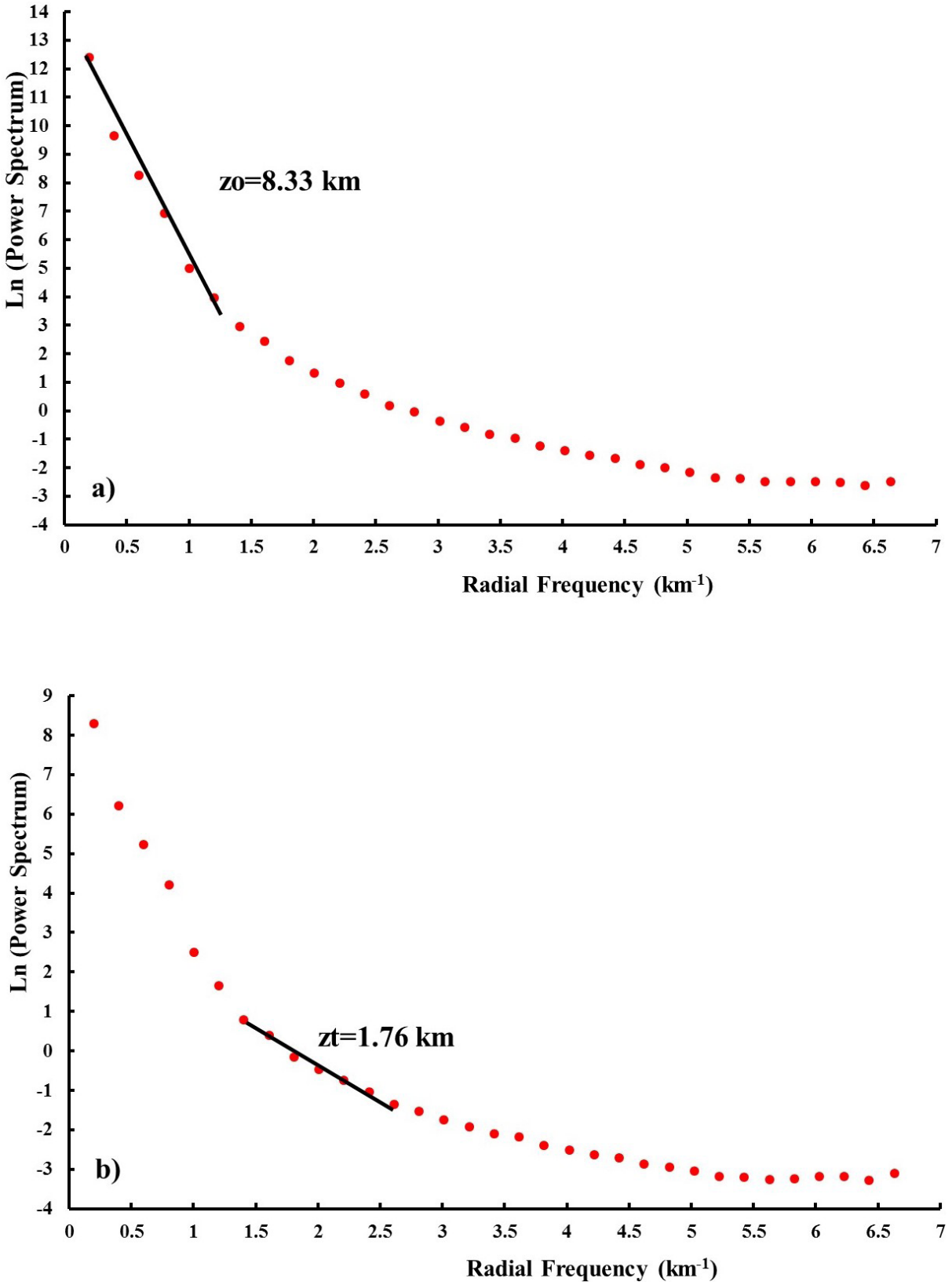

Figure 17. The power spectrum of the block-4 for estimation of the CPD, a) the determining of the centroid depth, z0, b) the determining of the top depth, zt.

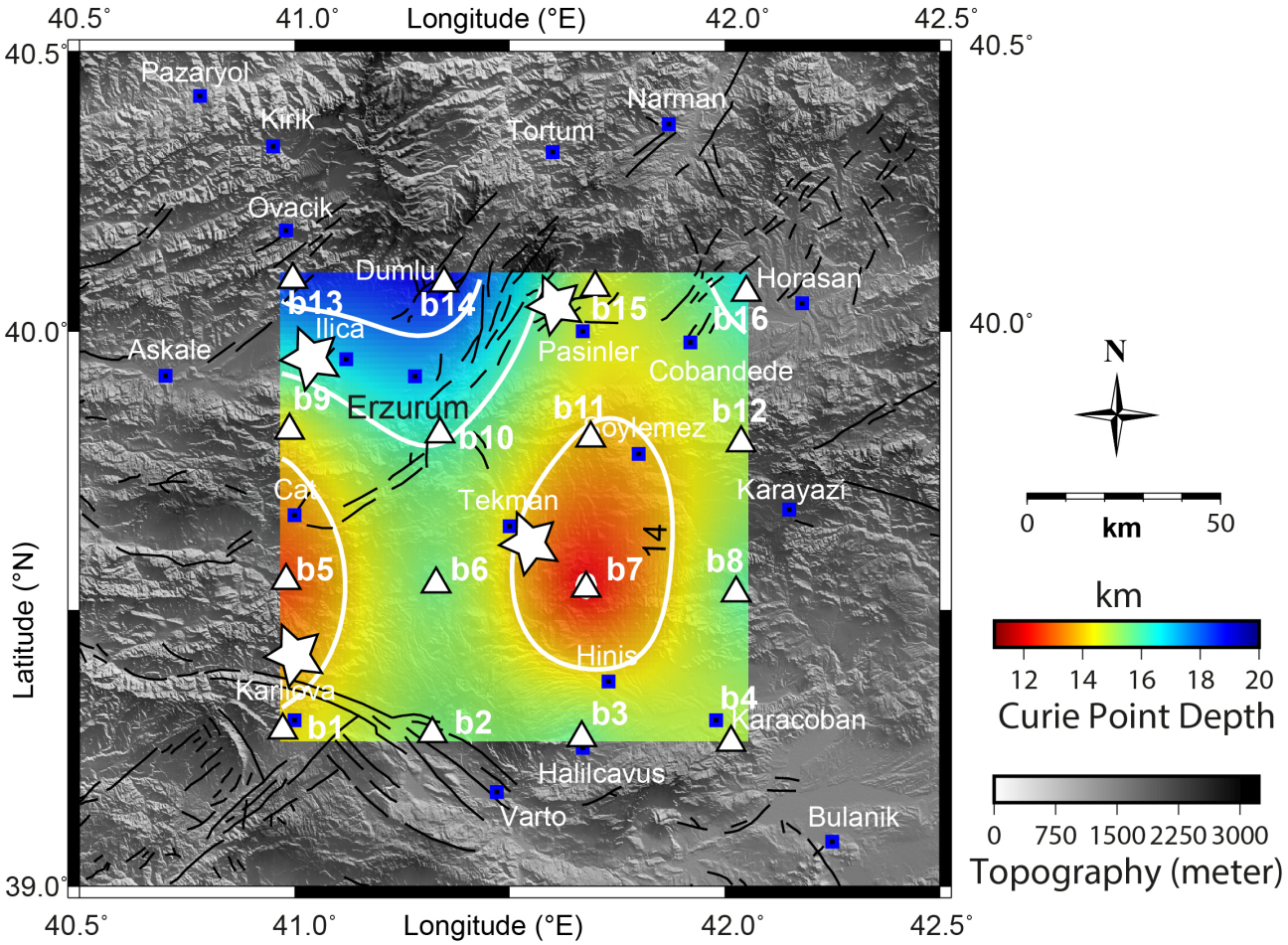

Figure 18. Curie point depth map for the study area. Triangle and star symbols show the blocks' centers of CPD block and hot spring points; respectively. The hot spot is reported by Akin et al. (2014) and MTA (2021). The black lines show tectonic units of the study area (Emre et al., 2013; 2018).

CPD values range from 11.73 to 19.8 (Table 2, Figure 18). Shallow CPD values may be associated with thin crust, geothermal potential and young volcanism (Aydın and Oksum, 2010; Khojamli et al., 2016). The largest CPD values were obtained in the centre of Erzurum and its north. The CPD value is less than 15 km in Tekman, Söylemez, Karlıova, Çat regions, (Figure 18). Shallower CPD values were obtained in B3, B7, B11 and B15 blocks than previous studies (Table 2).

4. Discussions

Bektas et al. (2007) reported that Curie point depths (CPDs) ranged from 18 km to 19 km in Erzurum using aeromagnetic data. The CPD of about 20 km is generally observed in the Erzurum according to Aydin et al. (2005). Pamukcu et al. (2014) claim that the CPD values vary from 12 to 16 km within the study coordinates. While the CPD values are 20 km in the northwest of the study area, it decreases to 12 km in Tekman and Karlıova regions. In Ilıca and Pasinler regions, where low enthalpy hot springs of Erzurum are located, the CPD values are calculated as 16 km. Considering these values, much higher hot enthalpy sources can be found in Tekman and between Karlıova and Çat regions. Another important finding supporting this idea is the low Vp values and high Vp / Vs ratios observed in these regions. Also, Yuce and Taskiran (2013) pointed to sources where the temperature may be 192 °C as a result of the interaction of mantle-based liquids to shallow layers in the study they conducted in Tekman-Erzurum. Alacali (2018) claimed that the maximum reservoir temperature they calculated using a chemical geothermometer could be 250 °C for the Erzurum region. Ozer and Ozyazicioglu (2019) interpreted Vp and Vp / Vs models together by using earthquake data from 2007 to 2017 in a local earthquake tomography study including Erzurum region and highlighted potential regions that could point to geothermal systems. In these regions, the variation of the Vp values area between –5% and –8% for depths of 10– 20

km. Vp / Vs ratio values vary between 1.6 and 2.0. The CPD values are less than 13 km especially in the regions between Hınıs, Söylemez, Tekman and Karayazı; and between Karlıova and Çat. The variation of Vp value for 10–20 km depths is between –5% and 5% in the region between Hınıs, Söylemez, Tekman, and Karayazı, and between –10 % and 0 % in the region between Karlıova and Çat. In the region between Hınıs, Söylemez, Tekman, and Karayazı, Vp / Vs values vary between 1.8 and 2. In the region between Karlıova and Çat, Vp / Vs values vary between 1.6 and 1.8. Considering study area, relatively low CPD values were characterized by high Vp / Vs ratio values. These areas need to be examined in detail for geothermal potential using magnetotelluric (MT) studies.

Sengor et al. (2003) showed that most of the East Anatolian High Plateau has not mantle lithosphere and not based on by thick crust, but by hot mantle. Zor et al. (2003) reported that the Anatolian has a remarkable low velocity zone. Zor (2008) exhibited the upper mantle negative velocity anomaly to deeper part of the EAR presumably related to the partially shallow molten asthenosphere. Ozer et al. (2019) claimed that the negative seismic velocity values in deep parts are associated with the hot mantle effect. Medved et al. (2021) reported that a wedge-shaped low-velocity structure exists in the lower crust. It was also observed that the seismic velocities decreased radically, especially after 20 km depth in this study.

The CPD values and the boundaries of the geological structures obtained by the tilt angle method were compared with the epicenter distributions of the earthquakes that occurred in the study. Erzurum center, Dumlu, Ilıca regions obtained with high CPD values were characterized by high seismic activity, and lower seismic activity was determined in the region between Hınıs, Söylemez, Tekman, and Karayazı where low CPD values were observed. Similarly, in the region between Çat and Karlıova with less seismic activity, CPD values are relatively lower. This situation can be explained by the complex geological and tectonic situation in the study area. It is known that the zero contours in the TA map directly point to the geological structure boundaries (fault, geological contact, etc.). It is observed that the earthquake epicentre distributions and faults in the northwest of the study area (Ovacık, Tortum, Narman) are NE - SW directional. The continuity of the faults in these areas is supported by earthquake epicenter distributions and the NE - SW directional structural boundaries determined by the TA method. The strike of the faults and the direction of the structure boundaries obtained by the TA method are compatible in this seismically active region, which is located in the SW of the study area.

It is difficult to say that there is a direct relationship between Vp and Vp / Vs horizontal models compared to b - values. But still, promising conformity, with low Vp velocities at depths of 0.5 and 10 km and high b - values indirectly points to the same meaning. High b - value and low Vp values can be evaluated from weakness zones in the region and for areas where potential earthquakes are expected (Ogata et al., 1991). Ogata et al. (1991) stated that the changes in b - value are compatible with the variations in seismic wave fractional velocity perturbations. They suggested that the areas with low and high values are related to the higher and lower parts of the P - wave velocity, respectively. Also, Öztürk (2017) performed a region-time evaluation of earthquake potential in the EAR of Turkey. In this study, spatial distribution of b - value as a function of time in the EAR was mapped for the time periods from 2002 to 2010 and from 2011 to 2015. One of the regions exhibiting large decreases in *b* - value (region B in Öztürk, 2017) cover the low *b* - value areas in the present study. As seen in Figure 10, these regions covering Pasinler, Söylemez, Horosan, Narman and Karayazı have relatively lower *b* - values smaller than 1.0. In addition, similar changes as in Ogata et al. (1991) were shown between regional distributions of *b* - value and Vp value. Upon the comparison of Vp - 0 km horizontal slice and magnetic anomaly map, conformity is found in the triangle area between Aşkale, Ilıca-Dumlu-Pasinler, and Narman and Karaçoban areas with low velocities and high magnetic anomaly values. There is also a significant adaptation between Vp values and magnetic anomaly. Similar inclusions exist in low Vp and high magnetic anomaly areas. These areas are Ilıca, Dumlu, Narman, Çobandede and Karaçoban. Similarly, high Vp and low magnetic anomaly inclusions are also conformable in Çat and Tekman. The low Vp and high magnetic anomaly inclusions of the N - W of Aşkale, Ilıca, Dumlu, Narman, Çobandede, Karaçoban, and southeast of Karlıova are very similar. There is no clear correlation between tilt angle and Vp models.

Consequently, a combined evaluation of the parameters such as *b*- value in the Gutenberg–Richter relation, Curie Point Depth and Vp / Vs ratio may be the key for a successful definition of the tectonic and structural characteristics of Erzurum and its surroundings (Eastern Turkey). However, a detailed study of geophysical data with high quality can be supplied as an improvement for the geodynamic processes of the crust. Considering the present data and parameters utilized in this study, obtained results should be supported with some other geophysical parameters to strengthen to findings. Also, when compared the results of this study with the literature studies, it can be clearly seen that the results of spatial distributions of the mentioned parameters in this study are similar with the results of the related other studies. Thus, the earthquake dataset and anomaly regions of the mentioned parameters in this study are more up-to-date and suitable with the literature.

5. Conclusion

This study presents a comprehensive analysis focused on the *b* - value, magnetic anomaly, CPD, tilt angle, total horizontal derivative, P-wave velocity change (Vp) and Vp / Vs ratio in order to uncover the tectonic and geothermal characteristics in the Erzurum region, Eastern Anatolia. A correlation of these parameters contributes to a better understanding of seismo-tectonic and structural properties in this region of Turkey. Some geothermal areas indicate the compatibility of tomographic anomalies, Curie point depths, *b* - values, and magnetic analysis reveals that the regions with negative Vp value and high Vp / Vs ratio are proportional to shallow Curie point depths and vice versa. We obtained high RTP total magnetic anomaly and low Vp values trending along the tectonically active regions; the Vp anomaly characteristic becomes negative toward the tectonic margins, suggesting a weakness zone of Erzurum such as Ilıca, Dumlu, Pasinler, Çat, Karlıova, and Karaçoban. The negative Vp characteristics with high *b* - values that trend mainly along from weakness zones from 0 to 10 km and for areas where potential earthquake hazard is high. Since the low Vp and high b - values in Karlıova, Karaçoban, Söylemez, Dumlu, Ilıca, Aşkale, and Kırık regions show that the seismic hazard in the region is high, engineering seismology studies are needed in these areas. Additional geophysical studies such as seismic reflection, magnetotellurics (MT), etc. are required to uncover the geothermal capacity of Tekman, Söylemez, the northern part of Karlıova, Karaçoban, Pasinler, and Ilıca regions.

Acknowledgment

Some images are created using ZMAP and GMT (Wiemer, 2001; Wessel et al., 2013). High-resolution topography and bathymetry data sets have been compiled from NOAA National Geophysical Data Center (NGDC, 2006) and Digital Elevation Model from United States Geological Survey (USGS, 1997). Tectonic units are digitized in the Geoscience map viewer and drawing editor licensed to the General Directorate of Mineral Research and Exploration (MTA) (Emre et al., 2013; 2018). The earthquake data were collected in SEISAN software (Havskov and Ottemoller, 1999).

References

Abdelfattah AK, Jallouli C, Qaysi S, Al-Qadasi B (2020). Crustal Stress in the Northern Red Sea Region as Inferred from Seismic b-values, Seismic Moment Release, Focal Mechanisms, Gravity, Magnetic, and Heat Flow Data. Surveys in Geophysics 41: 963-986.

Aki K (1965). Maximum likelihood estimate of b in the formula and its confidence limits. Bulletin of the Earthquake Research Institute Tokyo University 43: 237-239.

Akin U, Ulugergerli E, Kutlu S (2014). The assessment of geothermal potential of Turkey by means of heat flow estimation. Bulletin of the Mineral Research and Exploration 149: 201-210.

Alacali (2018). Hydrogeochemical investigation of geothermal springs in Erzurum, East Anatolia (Turkey). Environmental Earth Sciences 77: 802.

Ambraseys NN, Jackson JA (2000). Seismicity of the Sea of Marmara (Turkey) since 1500. Geophysical Journal International 141 (3): 1-6.

Ansari S (2016). Co-seismic stress transfer and magnitude-frequency distribution due to the 2012 Varzaqan-Ahar twin earthquakes (Mw 6.5 and 6.4), NW Iran. Journal of Asian Earth Sciences 132: 129-137.

Arkani-Hamed L (1988). Differential reduction to the pole or regional magnetic anomalies. Geophysics 53 (12): 1529-1600.

Arkani-Hamed L (2007). Differential reduction to the pole: Revisited. Geophysics 72 (1): 13-20.

Aydin I, Karat HI, Kocak A (2005). Curie-point depth map of Turkey. Geophysical Journal International 162 (2): 633-640.

Aydin I, Oksum E (2010). Exponential approach to estimate the Curie temperature depth. Journal of Geophysics and Engineering 7: 113-125.

Bayrak Y, Öztürk S, Çinar H, Kalafat D, Tsapanos TM et al. (2009). Estimating earthquake hazard parameters from instrumental data for different regions in and around Turkey. Engineering Geology 105: 200-210.

Bektas O, Ravat D, Buyuksarac A, Bilim F, Ates A (2007). Regional geothermal characterisation of East Anatolia from aeromagnetic, heat flow and gravity data. Pure and Applied Geophysics 164 (5): 975-998.

Bozkurt E (2001). Neotectonics of Turkey-a synthesis. Geodinamica Acta 14: 3-30.

Bulut F, Bohnhoff M, Eken T, Janssen C, Kılıç T et al. (2012). The East Anatolian Fault Zone: Seismotectonic setting and spatiotemporal characteristics of seismicity based on precise earthquake locations. Journal of Geophysical Research: Solid Earth 117 (B7).

Cao A, Gao SS (2002). Temporal variation of seismic b - value beneath north Eastern Japan island arc. Geophysical Research Letters 29 (48): 1-3.

Cordell L, Grauch VJS (1985). Mapping basement magnetization zones from aeromagnetic data in the San Juan Basin, New Mexico. In The utility of regional gravity and magnetic anomaly maps. Society of Exploration Geophysicists 181-197.

De´verche`re J, Petit C, Gileva N, Radziminovitch N, Melnikova V et al. (2001). Depth distribution of earthquakes in the Baikal rift system and its implications for the rheology of the lithosphere. Geophysical Journal International 146: 714-730.

Dewey JF, Hempton MR, Kidd WSF, Saroglu F, Sengor AMC (1986). Shortening of continental lithosphere: The neo-tectonics of eastern Anatolia- a young collision zone. In MP Coward, AC Reis (Eds.), Collision tectonics 3-36. London: Geological Society.

Dilek Y, Sandvol E (2009). Seismic structure, crustal architecture and tectonic evolution of the Anatolian-African plate boundary and the Cenozoic orogenic belts in the Eastern Mediterranean region. Geological Society, London, Special Publications 327 (1): 127-160.

Duman TY, Emre Ö (2013) The East Anatolian Fault: geometry, segmentation and jog characteristics. In: Geological Society, London, Special Publications. pp 495–529

El-Bohoty M, Brimich L, Saleh A, Saleh S (2012). Comparative study between the structural and tectonic situation of the Southern Sinai and the Red Sea, Egypt, as deduced from magnetic, gravity and seismic data. Contributions to Geophysics and Geodesy 42 (4): 357-388.

Emre O, Duman TY, Ozalp S, Elmaci H, Olgun S et al. (2013). 1/1.125.000 scale Active Fault Map of Turkey. General Directorate of Mineral Research and Explorations Special Publications Series, Ankara-Turkey. http://www.mta.gov.tr/v3.0/. Accessed 17 January 2021.

Emre O, Duman TY, Ozalp S, Saroglu F, Olgun S et al. (2018). Active fault database of Turkey. Bulletin of Earthquake Engineering 16: 3229-3275.

Fagereng A (2001). Frequency-size distribution of competent lenses in a block-in-matrix me´lange: imposed length scales of brittle deformation? Journal of Geophysical Research 116: B05302.

Frohlich C, Davis S (1993). Teleseismic b - values: Or, much ado about 1.0. Journal of Geophysical Research 98 (B1): 631-644.

Gok R, Pasyanos ME, Zor E (2007). Lithospheric structure of the continent-continent collision zone: Eastern Turkey. Geophysical Journal International 169: 1079-1088.

Gutenberg R, Richter CF (1944). Frequency of earthquakes in California. Bulletin of the Seismological Society of America 34: 185-188.

Habermann RE (1983). Teleseismic detection in the Aleutian Island arc. Journal of Geophysical Research 88 (B6): 5056-5064.

Hauksson E (2000). Crustal structure and seismicity distribution adjacent to the Pacific and North America plate boundary in southern California. Journal of Geophysical Research 105: 13875.

Havskov J, Ottemoller L (1999). SeisAn Earthquake analysis software. Seismological Research Letters 70 (55): 532-534.

Italiano F, Sasmaz A, Yuce G, Okan OO (2013). Thermal fluids along the East Anatolian Fault Zone (EAFZ): Geochemical features and relationships with the tectonic setting. Chemical Geology 339: 103-114.

Kalyoncuoglu UY, Elitok Ö, Dolmaz MN (2013). Tectonic implications of spatial variation of b - values and heat flow in the Aegean region. Marine Geophysical Research 34 (1): 59-78.

Kaygusuz A, Aslan Z, Aydıncakır E, Yucel C, Gucer MA et al. (2018). Geochemical and Sr-Nd-Pb isotope characteristics of the Miocene to Pliocene volcanic rocks from the Kandilli (Erzurum) area, Eastern Anatolia (Turkey): Implications for magma evolution in extension-related origin. Lithos 296: 332-351.

Kaypak B (2008). Three-dimensional VP and VP / VS structure of the upper crust in the Erzincan basin (eastern Turkey). Journal of Geophysical Research: Solid Earth 113 (7): 20.

Kaypak B, Gokkaya G (2012). 3 - D imaging of the upper crust beneath the Denizli geothermal region by local earthquake tomography, western Turkey. Journal of Volcanology and Geothermal Research 211-212: 47-60.

Keskin M, Pearce JA, Kempton PD, Greenwood P (2006). Magma-crust interactions and magma plumbing in a post-collisional setting: Geochemical evidence from the Erzurum- Kars volcanic plateau, eastern Turkey. Geological Society of America Special Paper 409: 475-505.

Ketin İ (1976). San Andreas ve Kuzey Anadolu Fayları arasında bir karşılaştırma. Türkiye Jeoloji Kurumu Bülteni 19: 149-154.

Khan PK, Chakraborty PP (2007). The seismic b - value and its correlation with Bouguer gravity anomaly over the Shillong Plateau area: Tectonic implications. Journal of Asian Earth Sciences 29: 136-147.

Khojamli A, Ardejani FD, Moradzadeh A, Kalate AN, Kahoo AR et al. (2016). Estimation of Curie point depths and heat flow from Ardebil province, Iran, using aeromagnetic data. Arabian Journal of Geosciences 9 (5): 383.

Kocyigit A, Canoglu MC (2017). Neotectonics and seismicity of Erzurum pull-apart basin, East Turkey. Russian Geology and Geophysics 58: 99-122.

Koulakov I (2009). LOTOS code for local earthquake tomographic inversion: Benchmarks for testing tomographic algorithms. Bulletin of the Seismological Society of America 99 (1): 194-214.

Idárraga-García J, Vargas CA (2018). Depth to the bottom of magnetic layer in South America and its relationship to Curie isotherm, Moho depth and seismicity behavior. Geodesy and Geodynamics 9 (1): 93-107.

Le Pichon X, Chamot-Rooke N, Lallemant S (1995). Geodetic determination of the kinematics of central Greece with respect to Europe: Implications for eastern Mediterranean tectonics. Journal of Geophysical Research 100: 12.675-12.690.

Le Pichon X, Kreemer C (2010) The miocene-to-present kinematic evolution of the eastern mediterranean and middle east and its implications for dynamics. Annual Review of Earth and Planetary Sciences 38 (1): 323-351.

Lee WHK, Lahr JC (1975). HYPO71 (Revised): A Computer Program for Determining Hypocenter, Magnitude, and First Motion Pattern of Local Earthquakes. U.S. Geological Survey Open File Report 75-311, 113.

Li CF, Lu Y, Wang J (2017). A global reference model of Curie-point depths based on EMAG2. Scientific reports 7 (1): 1-9.

Maden N (2012). One-dimensional thermal modelling of the eastern pontides orogenic belt (NE Turkey). Pure and Applied Geophysics 169: 235-248.

Maden N, Aydin A, Kadirov F (2015). Determination of the crustal and thermal structure of the Erzurum-Horasan-Pasinler Basins (Eastern Turkiye) using gravity and magnetic data. Pure and Applied Geophysics 172: 1599-1614.

Maden N, Öztürk S (2015). Seismic *b* - values, Bouguer gravity and heat flow data beneath Eastern Anatolia, Turkey: Tectonic implications. Survey in Geophysics 36: 549-570.

Maus S, Barckhausen U, Berkenbosch H, Bournas N, Brozena J et al. (2009). EMAG2: A 2-arc min resolution Earth Magnetic Anomaly Grid compiled from satellite, airborne, and marine magnetic measurements. Geochemistry, Geophysics, Geosystems 10 (8).

McClusky S, Balassanian S, Barka A, Demir C, Ergintav S et al. (2000). Global Positioning System constraints on plate kinematics and dynamics in the eastern Mediterranean and Caucasus. Journal of Geophysical Research 105: 5695-5719.

McKenzie D (1976). The east Anatolian fault: A major structure in eastern Turkey. Earth and Planetary Science Letters 29: 189-193.

Medved I, Polat G, Koulakov I (2021). Crustal Structure of the Eastern Anatolia Region (Turkey) Based on Seismic Tomography. Geosciences 11 (2): 91.

Mignan A, Woessner J (2012). Estimating the magnitude of completeness for earthquake catalogs. Community Online Resource for Statistical Seismicity Analysis. doi: 10.5078/corssa-00180805. Available at http://www.corssa.org.

Miller HG, Singh V (1994). Potential field tilt - a new concept for location of potential field sources. Journal of Applied Geophysics 32: 213-217.

Mogi K (1962). Magnitude-frequency relation for elastic shocks accompanying fractures of various materials and some related problems in earthquakes. Bulletin of the Earthquake Research Institute, Tokyo University 40: 831-853.

MTA (2021). General Directorate of Mineral Research and Explorations. www.mta.gov.tr. Accessed 17 January 2021.

Njeudjang K, Kana JD, Tom A, Essi JMA, Djongyang N et al (2020). Curie point depth and heat flow deduced from spectral analysis of magnetic data over Adamawa volcanic region (Northern Cameroon): geothermal implications. SN Applied Sciences 2 (8): 1-16.

NGDC (2006). Two-minute gridded global relief data (ETOPO2) v2. National Geophysical Data Center (NGDC), NOAA, doi: 10.7289/V5J1012Q.

Ogata Y, Imoto M, Katsura K (1991). 3 - D spatial variation of b - values of magnitude-frequency distribution beneath the Kanto District, Japan. Geophysical Journal International 104: 135-146.

Oruç B, Sertcelik I, Kafadar O, Selim HH (2013). Structural interpretation of the Erzurum Basin, eastern Turkey, using curvature gravity gradient tensor and gravity inversion of basement relief. Journal of Applied Geophysics 88: 105-113.

Oruç B, Selim HH (2011). Interpretation of magnetic data in the Sinop area of Mid Black Sea, Turkey, using tilt derivative, Euler deconvolution, and discrete wavelet transform. Journal of Applied Geophysics 74 (4): 194-204.

Okubo Y, Graf RJ, Hansen RO, Ogawa K, Tsu H (1985). Curie-point depths of the Island of Kyushu and surrounding areas, Japan. Geophysics 50 (3): 481-494.

Ozer C, Polat O (2017). 3 - D crustal velocity structure of Izmir and surroundings. Journal of the Faculty of Engineering and Architecture of Gazi University 32(3): 733-747.

Ozer C (2019). Determination of 3 - D crustal seismic velocity structure beneath Hatay and surroundings. Journal of the Faculty of Engineering and Architecture of Gazi University 34(4): 2215-2227.

Ozer C, Ozyazicioglu M (2019). The Local Earthquake Tomography of Erzurum (Turkey) Geothermal Area. Earth Sciences Research Journal 23(3): 209-223.

Ozer C, Ozyazicioglu M, Gok E, Polat O (2019). Imaging the Crustal Structure Throughout the East Anatolian Fault Zone, Turkey, by Local Earthquake Tomography. Pure and Applied Geophysics 176 (6): 2235- 2261.

Öztürk S (2009). An application of the earthquake hazard and aftershock probability evaluation methods to Turkey earthquakes. PhD Thesis, Karadeniz Technical University, Trabzon, Turkey (in Turkish with English abstract).

Öztürk S (2017). Space-time assessing of the earthquake potential in recent years in the eastern Anatolia region of Turkey. Earth Sciences Research Journal 21 (2): 67-75.

Öztürk S (2018). Earthquake hazard potential in the Eastern Anatolian region of Turkey: seismotectonic *b* and *Dc*-values and precursory quiescence *Z*-value. Frontiers in Earth Science 12 (1): 215-236.

Öztürk S, Sahin S (2019). A statistical space-time-magnitude analysis on the aftershocks occurrence of the July 21th, 2017 M_W = 6.5 Bodrum-Kos, Turkey, earthquake. Journal of Asian Earth Sciences 172: 443-457.

Pamuk E (2019). Investigating edge detection, Curie point depth, and heat flow using EMAG2 magnetic and EGM08 gravity data in the northern part of Eastern Anatolia, Turkey. Turkish Journal of Earth Sciences 28 (6): 805-821.

Pamukcu O, Akcig Z, Hisarli M, Tosun S (2014). Curie Point depths and heat flow of eastern Anatolia (Turkey). Energy Sources. Part A: Recovery, Utilization, and Environmental Effects 36 (24): 2699-2706.

Reilinger RE, McClusky SC, Oral MB, King RW, Toksöz MN et al. (1997). Global Positioning System measurements of present-day crustal movements in the Arabia-Africa-Eurasia plate collision zone. Journal of Geophysical Research 102 (B5): 9983-9999.

Salem A, Williams S, Fairhead JD, Ravat D, Smith R (2007). Tilt-depth method: A simple depth estimation method using first-order magnetic derivatives. The leading Edge 26 (12): 1502-1505.

Sanchez JJ, McNutt SR, Power JA, Wyss M (2004). Spatial variations in the frequency-magnitude distribution of earthquakes at Mount Pinatubo volcano. Bulletin of the Seismological Society of America 94: 430-438.

Scholz CH (1968). The frequency-magnitude relation of microfracturing in rock and its relation to earthquakes. Bulletin of the Seismological Society of America 58: 399-415.

Schorlemmer D, Wiemer S, Wyss M (2005). Variations in earthquake-size distribution across different stress regimes. Nature 437.

Simao NM, Nalbant SS, Sunbul F, Mutlu AK (2016). Central and eastern Anatolian crustal deformation rate and velocity fields derived from GPS and earthquake data. Earth and Planetary Science Letters 433: 89-98.

Spector A, Grant FS (1970). Statistical models for interpreting aeromagnetic data. Geophysics 35 (2): 293-302.

Sengor AMC, Ozeren S, Genc T, Zor E (2003). East Anatolian high plateau as a mantle-supported, north-south shortened domal structure. Geophysical Research Letters 30 (24): 8045.

Şengör AMC, Tüysüz O, İmren C, Sakınç M, Eyidoğan H et al. (2004). The North Anatolian Fault: A New Look. Annual Review of Earth and Planetary Sciences 33: 37-112.

USGS (1997). Earth Resources Observation and Science Center/U.S. Geological Survey/U.S. Department of the Interior. USGS 30 ARC-second Global Elevation Data, GTOPO30. Research Data Archive at the National Center for Atmospheric Research, Computational and Information Systems Laboratory.

Utsu T (1971). Aftershock and earthquake statistic (III): Analyses of the distribution of earthquakes in magnitude, time and space with special consideration to clustering characteristics of earthquake occurrence. Journal of Faculty of Science Hokkaido University Series VII (Geophysics) 3: 379-441.

Zor E, Sandvol E, Gurbuz C, Turkelli N, Seber D et al. (2003). The crustal structure of the East Anatolian plateau (Turkey) from receiver functions. Geophysical Research Letters 30 (24): 8044.

Zor E (2008). Tomographic evidence of slab detachment beneath eastern Turkey and the Caucasus. Geophysical Journal International 175: 1273-1282.

Wang JH (1988). b - values of shallow earthquakes in Taiwan. Seismological Society of America Bulletin 66: 1243-1254.

Wessel P, Smith WHF, Scharroo R, Luis JF, Wobbe F (2013). Generic Mapping Tools: Improved version released. EOS Transactions American Geophysical Union 94: 409-410.

Westeway R (1994). Present-day kinematics of the Middle East and Eastern Mediterranean. Journal of Geophysical Research 99: 12071-12090.

Wiemer S (2001). A software package to analyze seismicity: ZMAP. Seismological Research Letters 72 (3): 373–382.

Wiemer S, McNutt SR, Wyss M (1998). Temporal and three-dimensional spatial analyses of the frequency–magnitude distribution near Long Valley Caldera, California. Geophysical Journal International 134: 409-421.

Wiemer S, Katsumata K (1999). Spatial variability of seismicity parameters in aftershock zones. Journal of Geophysical Research 104 (B6): 13135-13151.

Wiemer S, Wyss M (2000). Minimum magnitude of completeness in earthquake catalogs: Examples from Alaska, the Western United States, and Japan. Bulletin of the Seismological Society of America 90 (3): 859-869.

Woessner J, Wiemer S (2005). Assessing the quality of earthquake catalogues: Estimating the magnitude of completeness and its uncertainty. Bulletin of the Seismological Society of America 95 (2): 684-698.

Wong HK, Degens ET, Finckh P (1978). Structures in modern Lake Van sediments as revealed by 3.5 KHz high resolution profiling. In: E.T. Degens and F. Kurtman (eds.), Geology of Lake Van, Bulletin of the Mineral Research and Exploration 169: 11-19.

Yuce G, Taskiran L (2013). Isotope and chemical compositions of thermal fluids at Tekman Geothermal Area (Eastern Turkey). Geochemical Journal 47: 423-435.

Xu Y, Hao T, Zeyen H, Nan F (2017). Curie point depths in North China Craton based on spectral analysis of magnetic anomalies. Pure and Applied Geophysics 174 (1): 339-347.